TRIUMF

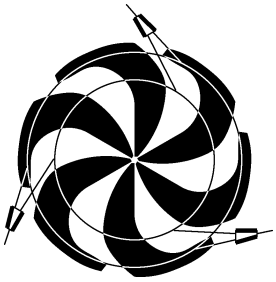

ANNUAL REPORT
SCIENTIFIC ACTIVITIES
1999

ISSN 1492-417X

CANADA'S NATIONAL LABORATORY
FOR PARTICLE AND NUCLEAR PHYSICS

OPERATED AS A JOINT VENTURE

MEMBERS:

THE UNIVERSITY OF ALBERTA
SIMON FRASER UNIVERSITY
THE UNIVERSITY OF VICTORIA
THE UNIVERSITY OF BRITISH COLUMBIA

ASSOCIATE MEMBERS:

CARLETON UNIVERSITY
THE UNIVERSITY OF MANITOBA
L'UNIVERSITÉ DE MONTRÉAL
QUEEN'S UNIVERSITY
THE UNIVERSITY OF REGINA
THE UNIVERSITY OF TORONTO

UNDER A CONTRIBUTION FROM THE
NATIONAL RESEARCH COUNCIL OF CANADA

JULY 2000

The contributions on individual experiments in this report are outlines intended to demonstrate the extent of scientific activity at TRIUMF during the past year. The outlines are not publications and often contain preliminary results not intended, or not yet ready, for publication. Material from these reports should not be reproduced or quoted without permission from the authors.

PARTICLE PHYSICS

Experiment 497
Measurement of the flavour conserving hadronic weak interaction

(J. Birchall, S.A. Page, W.T.H. van Oers, Manitoba)

The first experiment to measure parity violation in *pp* scattering at 221 MeV is now nearing completion at TRIUMF. The experiment uses hydrogen-filled ion chambers located upstream and downstream of a 400 mm liquid hydrogen target to measure the dependence of the *pp* elastic cross section on the helicity of the incident beam, hence determining the parity-violating longitudinal analyzing power $A_z = (\sigma^+ - \sigma^-)/(\sigma^+ + \sigma^-)$, where σ^+ and σ^- are the scattering cross sections for positive and negative helicity. The experiment has now achieved a statistical precision of $\pm 0.2 \times 10^{-7}$ on A_z. Systematic uncertainties are dominated by corrections for first moments of transverse polarization and contribute an additional uncertainty of similar magnitude. Data analysis is currently under way for the last of 4 data sets: February, 1997, December, 1997-January, 1998, July-August, 1998, and May-June, 1999. It is expected that A_z will be determined to $\pm 0.3 \times 10^{-7}$ when both statistical and systematic uncertainties are included. To the extent that the interaction can be explained by meson exchange and that the strong phase shifts are known, the TRIUMF result depends only on the strength of the weak ρ-meson-nucleon-nucleon coupling, $h_\rho^{pp} = (h_\rho^0 + h_\rho^1 + h_\rho^2/\sqrt{6})$. This is because the beam energy and detector geometries have been selected [Simonius, Can. J. Phys. **66**, 548 (1988)] to ensure that only parity mixing in the ${}^3P_2 - {}^1D_2$ partial wave amplitude contributes to the measured parity violating asymmetry.

Experimental and theoretical developments confirm the importance of achieving high quality results from the TRIUMF experiment; a measurement of A_z at 13.6 MeV ($-0.93 \pm 0.20 \pm 0.05 \times 10^{-7}$) [Eversheim *et al.*, Phys. Lett. **B256**, 11 (1991); private communication (1994)] has reached the high level of accuracy reported earlier by the PSI group at 45 MeV ($-1.50 \pm 0.22 \times 10^{-7}$) [Kistryn *et al.*, Phys. Rev. Lett. **58**, 1616 (1987)]. The low energy data constrain the combination $(h_\rho + 0.7 h_\omega)$. Addition of a high quality result from the TRIUMF experiment is important to isolate h_ρ.

A major effort to minimize and understand systematic error contributions is required to successfully perform an experiment to this level of precision. The first significant data set for Expt. 497 was acquired in February, 1997, with a statistical error of $\pm 0.4 \times 10^{-7}$ and most systematic errors at or below the 10^{-7} level. That result represented a major milestone for the experiment, the culmination of many years of effort to reduce both the helicity correlated beam modulations Δx_i and the sensitivities $\frac{\partial A_z}{\partial x_i}$. Data-taking has continued with three more month-long runs acquired during 1998 and 1999.

Beam line and instrumentation

In addition to the measuring apparatus, the optically pumped polarized ion source (OPPIS), cyclotron, and transport beam lines are critical components of the experimental set-up, as illustrated in Fig. 1. A 5 μA transversely polarized beam is transported to the cyclotron through an approximately 50 m long injection beam line. The ion source Wien filter is tuned to produce vertical polarization at the entrance to the cyclotron. A 200 nA beam at 75–80% vertical polarization is extracted at 221 MeV. Spin precession through a pair of solenoid and dipole magnets results in delivery of a longitudinally polarized beam to the 400 mm liquid hydrogen target, which scatters 4% of the beam. Transverse field parallel plate ion chambers, TRIC1 and TRIC2, measure the beam current upstream and downstream of the target. The parity violation signal is derived from the helicity-correlated difference between the beam currents measured by the two TRICs. Upstream of the target are two polarization profile monitors (PPMs) to measure the distributions of transverse polarization $P_y(x)$ and $P_x(y)$ across the beam. Two fast intensity profile monitors (IPMs) measure the intensity distribution of beam current in x and y and are coupled to a pair of servo magnets which lock the beam path on the optimum axis through the equipment. A third slower IPM is also available to assist in beam tuning.

Data

The full parity data set now consists of four major (1 month) data runs, taken in February, 1997, in December, 1997-January, 1998, July-August, 1998, and May-June, 1999. These runs have a raw statistical error of approximately $\pm 0.4 \times 10^{-7}$ each. In all cases, however, the precision of the final result is limited by corrections for systematic error. A major effort has been under way to analyze the recent data sets, and preliminary results are summarized in this report.

The longitudinal analyzing power A_z is deduced from each 8-state data cycle by forming the helicity-correlated digitized TRIC difference signal, multiplied by a scale factor appropriate to the electronic and gas gains etc., and divided by the average incident beam current measured by TRIC1. Ion chamber noise and random beam and cyclotron instabilities are largely responsible for the width of the A_z distribution (the normal 'counting statistics' contribution is negligible).

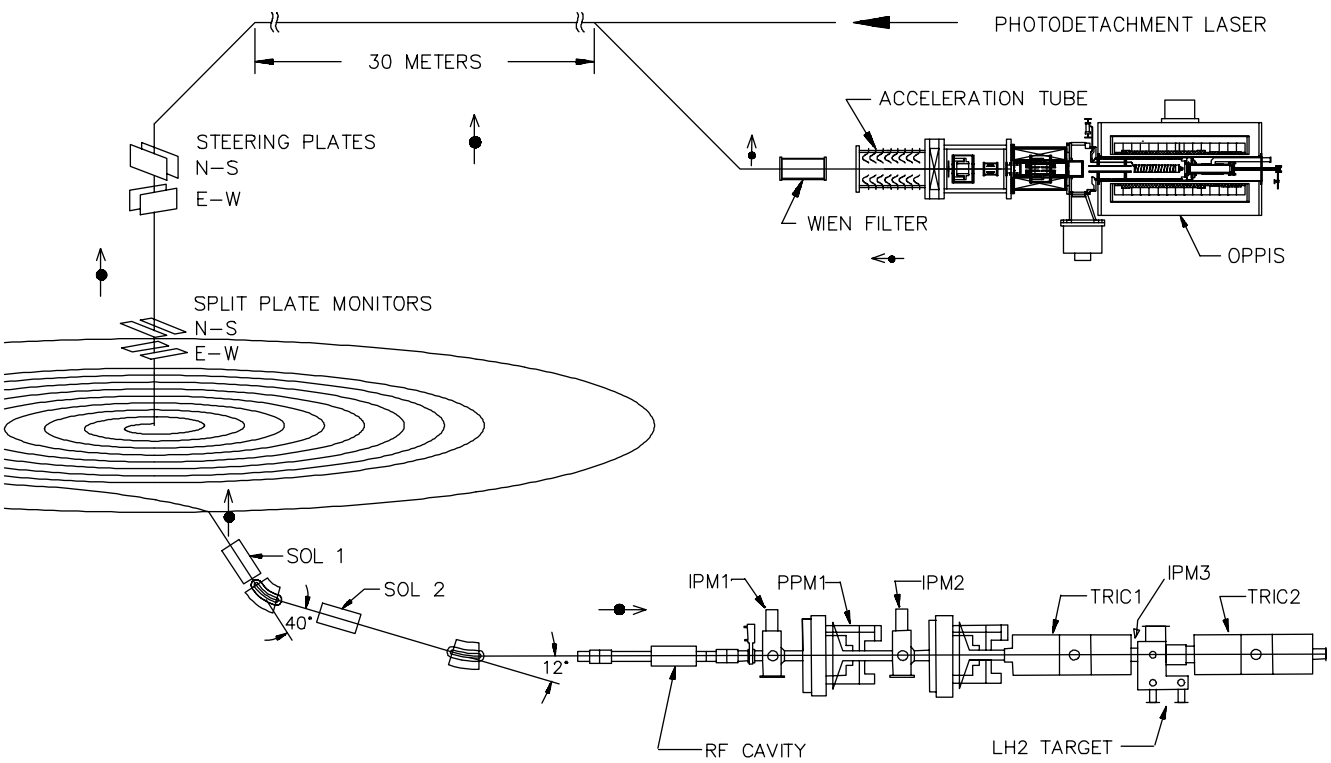

Fig. 1. General layout of the TRIUMF parity experiment. (OPPIS: optically pumped polarized ion source; SOL: spin precession solenoid; IPM: intensity profile monitor; PPM: polarization profile monitor; TRIC: transverse field ionization chamber).

The width is minimized by aligning the beam along the symmetry or 'neutral axis' of the apparatus and ensuring that the two TRICs are as identical as possible in their response to the beam. Helicity-correlated changes in beam properties other than longitudinal polarization give rise to systematic errors which shift the mean of the A_z distribution away from zero; these errors are studied in a series of calibration measurements in which small spin-state-correlated modulations of beam current, energy, position, angle, and transverse polarization are purposely introduced. Interspersed data acquired in the frequent spin-off cycles provide an important zero asymmetry check of the apparatus and electronics.

February, 1997 data

A thorough re-analysis of the February, 1997 data was reported last year [Hamian, Ph.D. thesis, Univ. of Manitoba (1998)]. The method described by Hamian has also been used for the analysis of all subsequent data sets. The dominant correction is due to the **intrinsic** moments of transverse polarization $\langle xP_y\rangle$ and $\langle yP_x\rangle$ resulting from a non-uniform distribution of transverse polarization within the beam envelope, as distinct from the corresponding **extrinsic** polarization moments $\langle x\rangle\langle P_y\rangle$ and $\langle y\rangle\langle P_x\rangle$ which arise when a beam with finite transverse polarization is displaced from the polarization neutral axis.

The polarization neutral axis, which defines $\langle x\rangle = 0$, $\langle y\rangle = 0$, is determined from routine calibration scans of the sensitivity to extrinsic polarization moments, several times per data run. These scans yield a set of coefficients which are used to correct the raw asymmetries for nonzero average polarization components $\langle P_y\rangle$ and $\langle P_x\rangle$. These extrinsic calibration coefficients also determine the optimum beam convergence at the LH_2 target to minimize the sensitivity to intrinsic polarization moments $\langle xP_y\rangle$ and $\langle yP_x\rangle$. The sensitivities of the apparatus to both intrinsic and extrinsic polarization moments are identical, so in principle only the extrinsic polarization scans are required to determine the sensitivity coefficients for both effects. However, since the resolution of the PPMs is significant compared to the intrinsic polarization moments that they measure, the corrections for intrinsic polarization moments made in this manner inflate the error bar on A_z significantly.

Corrections for intrinsic polarization moments can also be made by combining the extrinsic correction coefficients with measurements of the **ratio** of intrinsic moments at PPM1 and PPM2, i.e. $\langle xP_y\rangle_2/\langle xP_y\rangle_1$ and similarly for $\langle yP_x\rangle$, averaged over the entire parity data sample. This reduces the uncertainty in the overall correction, provided that the ratio is consistent over the data sample it is calculated from. The method is based

on the assumption that although the size of the first moments at PPM1 and PPM2 can vary from run to run, their ratio is controlled mainly by the beam line magnets and does not change. Extremely stable and reproducible beam tune conditions are needed over the course of a running period for the ratio method to work. The uncertainty in the overall correction using this method is reduced because the *effective* sensitivity obtained by scaling the extrinsic correction coefficients using the average intrinsic moment ratio is significantly smaller than the sensitivity at each PPM. (With the optimal intrinsic moments ratio, the effective sensitivity to intrinsic moments vanishes.)

Finally, corrections can be made for intrinsic polarization moments based on a regression analysis applied to the parity data. The procedure used is to first correct the experimental asymmetries for all other systematic effects, and then use regression to determine the correlation between the semi-corrected asymmetries and the intrinsic polarization moments. When the data are bundled into samples of 5000 or more event pairs (approx. 1/2 hour acquisition time), the intrinsic moment sensitivities obtained from the regression analysis are in agreement with the sensitivities obtained from the extrinsic coefficients scaled by the average ratio of intrinsic first moments measured by PPM1 and PPM2, but are determined with better precision.

The February, 1997 data were analyzed using these three different methods of correcting for the effects of first moments. The corrected A_z values are consistent in all 3 cases; the spread in the data is dramatically reduced using the regression technique. Note that, as does the ratio method, the regression analysis approach requires that the beam tune be constant over the entire set of runs, since it assumes a constant net intrinsic first moment sensitivity, while the approach based on extrinsic coefficients alone is beam tune independent. In any case, there is only one significant correction to the February, 1997 data, corresponding to the intrinsic first moment of transverse polarization $\langle xP_y \rangle$. The sensitivity coefficients for this correction are in agreement as determined by two independent methods – the regression analysis applied to the raw A_z data, and the extrinsic calibration method described earlier. The corrected A_z values have a reduced χ^2 of 0.5 per degree of freedom, as compared with 10.8 for the raw A_z values for the same 7 data sets. All other corrections are negligible on the 10^{-7} scale.

The agreement of data taken in different beam line helicity states and with different Wien filter settings, after being corrected for all measurable systematic errors, can be used to set upper limits on helicity correlated effects that are not measurable at the parity apparatus, such as energy modulation at the eV level in the extracted beam. The excellent consistency of the February, 1997 data after correcting for all known effects indicates that unmeasured systematic errors correlated with both the direction of spin at the ion source and the direction of spin in the cyclotron are consistent with zero at the level of precision in A_z, approximately $\pm 0.7 \times 10^{-7}$.

The mean value of A_z before systematic error corrections is $(1.1 \pm 0.5) \times 10^{-7}$; the final corrected result from the February, 1997 data set is found to be:

$$A_z = (0.33 \pm 0.57 \pm 0.31) \times 10^{-7} = (0.33 \pm 0.65) \times 10^{-7}$$

where the first error is derived from the standard deviation of the corrected A_z distribution ("statistical") and the second is the contribution from the uncertainties in the sensitivity coefficients ("systematic"). The statistical error includes the uncertainty in ΔA_z due to the spread of the helicity correlated beam property measurements, but is dominated by the spread of the raw A_z values. The systematic error, since it is due almost entirely to the uncertainty in the $\langle xP_y \rangle$ sensitivity as determined from the regression analysis of the parity data, is in fact statistics dominated.

December, 1997-January, 1998 data

During the December, 1997-January, 1998 running period, approximately 150 hours of polarized data were acquired in addition to systematic error calibrations and other tests. Although the liquid hydrogen target performed excellently, a failure of the HE2 probe control mechanism prevented the optimum cyclotron tune from being reestablished with the ultrathin stripping foil. Relatively large raw asymmetries obtained from the on-line analysis indicated that the beam convergence was not appropriate to reduce the intrinsic first moment sensitivity to zero, and extra time was spent experimenting with different beam tunes to ameliorate the situation.

The raw data have a statistical error of $\pm 0.4 \times 10^{-7}$ grouped into 14 main data sets according to the beam line helicity tune, but the consistency of the raw A_z values on a set-by-set basis is about an order of magnitude worse than this. Because the December-January data were acquired with a variety of beam tune conditions and two drastically different cyclotron stripping foils, the data sets do not have a consistent net sensitivity to intrinsic first moments of transverse polarization $\langle xP_y \rangle$ and $\langle yP_x \rangle$. For this reason, we cannot take advantage of the techniques applied to the February, 1997 data to reduce the uncertainty in the correction for intrinsic moments. Corrections for intrinsic polarization moments have only been made with the 'tune independent' method using external calibration sensitivities at each PPM. These preliminary results for the corrected A_z values are shown in Fig. 2. As seen in the

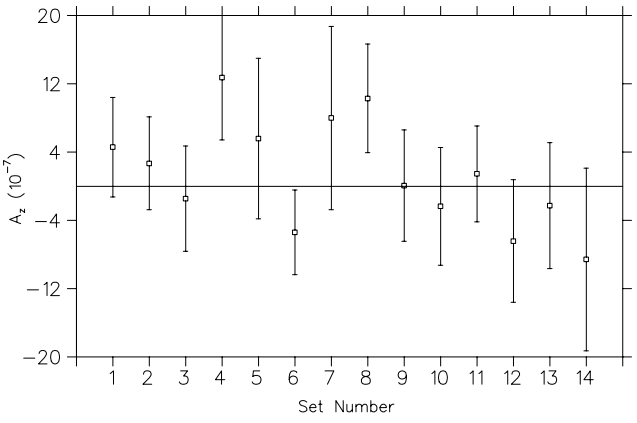

Fig. 2. Preliminary results for corrected A_z data from December, 1997-January, 1998, plotted versus set number. Corrections were made using the 'tune independent' method for intrinsic first moment sensitivities, which introduces additional noise in the corrected values.

figure, the corrected values are consistent with each other. A reduced χ^2 of 0.8 for 13 degrees of freedom results from this analysis, but unfortunately the correction introduces additional noise in each data set.

The preliminary result for the December-January data from this analysis is:

$$A_z = (0.8 \pm 1.8) \times 10^{-7}$$

where the error bar is dominated by the uncertainty in the correction for intrinsic polarization moments. No residual correlations of the corrected A_z are found with any other helicity correlated beam properties for these data, and the data are consistent with zero systematic offsets associated with the spin direction at the ion source and at the cyclotron stripping foil.

July-August, 1998 data

The July-August, 1998 data have been analyzed in the manner described above as applied to the February, 1997 data. The raw data are grouped into 9 sets according to beam line helicity tune, as shown in Fig. 3. The raw analyzing power is $A_z = (1.6 \pm 0.3) \times 10^{-7}$ with a reduced chisquared of 5; once again the largest correction to A_z is due to the intrinsic first moments, as discussed in detail below.

The intrinsic first moments corrections to the July-August, 1998 data are shown in Table I for the ratio method and the regression method. The statistical and systematic error bars are not suppressed and are shown separately for each correction. One clearly sees the larger error bars, both statistical and systematic, when using the ratio method as compared to the regression. Since the sensitivity for $\langle xP_y \rangle$ could not be reliably extracted using the regression method, none was used. As in February, 1997 the first moments are the largest correction to $A_z^{\rm raw}$ and also the largest source of uncertainty.

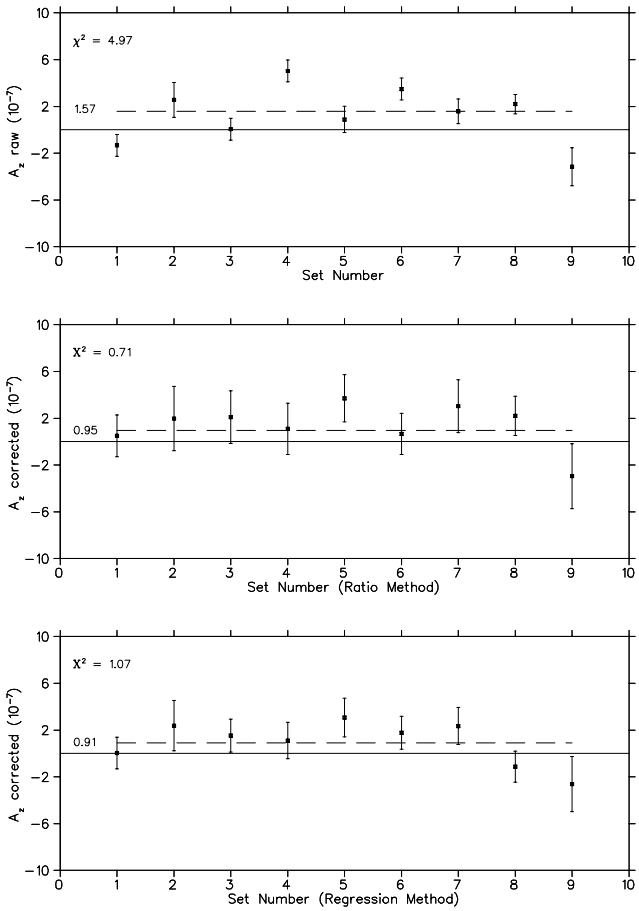

Fig. 3. (top) The raw analyzing power, (middle) corrected analyzing power using the ratio method to correct for intrinsic first moments, (bottom) corrected analyzing power using the regression first moment sensitivities.

Table I. The corrections for intrinsic first moments for the July-August, 1998 data as determined by the ratio method and the regression analysis. The regression method could not consistently extract a $\langle xP_y \rangle$ sensitivity and when extracted was consistent with zero. Subsequently no correction was used for $\langle xP_y \rangle$.

"+" Beam line helicity sets only (1,3,5,7,9)

Method	Moment	$10^7 \Delta A_z$
Ratio	$\langle yP_x \rangle$	$-1.67 \pm 0.07 \pm 1.31$
Ratio	$\langle xP_y \rangle$	$0.11 \pm 0.02 \pm 0.36$
Regression	$\langle yP_x \rangle$	$-1.08 \pm 0.04 \pm 0.37$
Regression	$\langle xP_y \rangle$	none used

"–" Beam line helicity sets only (2,4,6,8)

Method	Moment	$10^7 \Delta A_z$
Ratio	$\langle yP_x \rangle$	$-2.64 \pm 0.19 \pm 0.80$
Ratio	$\langle xP_y \rangle$	$1.99 \pm 0.26 \pm 0.73$
Regression	$\langle yP_x \rangle$	$-2.52 \pm 0.18 \pm 0.31$
Regression	$\langle xP_y \rangle$	none used

Table II. Summary of the A_z corrections other than the intrinsic first moments for the July, 1998 data.

Property	$10^7 \Delta A_z$	ΔA_z (+helicity)	ΔA_z (−helicity)
P_x	0.06 ± 0.01	0.17 ± 0.02	0.05 ± 0.02
P_y	-0.03 ± 0.01	-0.03 ± 0.01	0.02 ± 0.01
$\Delta I/I$	-0.01 ± 0.01	-0.01 ± 0.01	0.00 ± 0.01
$\Delta\sigma_x$	-0.04 ± 0.24	0.43 ± 0.31	0.50 ± 0.35
$\Delta\sigma_y$	-0.03 ± 0.24	-0.86 ± 0.32	-0.80 ± 0.35
Δx	0.00 ± 0.01	0.01 ± 0.01	0.00 ± 0.00
Δy	-0.02 ± 0.04	0.02 ± 0.07	0.07 ± 0.06
Total	-0.06 ± 0.34	-0.27 ± 0.45	-0.16 ± 0.49

Table II summarizes the correction to the July, 1998 $A_z^{\rm raw}$ data for all of the beam properties *other than* the intrinsic first moments. The corrections for the helicity correlated positions and extrinsic moments are in all cases small ($\leq 0.1 \times 10^{-7}$). The total correction due to everything but first moments is $0.06 \pm 0.34 \times 10^{-7}$. There is some cancellation that occurs between the beam line helicity sets that results in a small overall helicity correlated size correction. The largest error bar in these corrections is due to the helicity correlated sizes; the error bar is largely statistical and should decrease with the addition of other data sets.

The preliminary result for the July, 1998 data set uses the sensitivities derived from the external calibration data for the extrinsic moments and the helicity correlated positions and sizes. The first moment sensitivities are derived from the regression analysis. The raw analyzing power and the total correction are:

$$\begin{aligned} A_z^{\rm raw} &= (1.57 \pm 0.34) \times 10^{-7} \\ \Delta A_z &= (0.67 \pm 0.15 \pm 0.34) \times 10^{-7}\,. \end{aligned}$$

The preliminary result is:

$$A_z = (0.91 \pm 0.34 \pm 0.34) \times 10^{-7} = (0.91 \pm 0.48) \times 10^{-7}\,.$$

If one is more conservative and uses the ratio method to estimate the systematic uncertainty for $\langle x P_y \rangle$ then the total error bar increases to $\pm 0.95 \times 10^{-7}$. Figure 3 shows the progression from raw A_z to corrected A_z using the two main methods of correcting for the intrinsic first moments. The averages shown are the unweighted averages.

May-June, 1999 data

Nominally, Expt. 497 ran for five weeks from 19 May to 23 June, 1999. In practice, the run was plagued by so many technical problems that it was roughly equivalent to a two-week run. At the beginning of the run, 10 days were lost due to a failure of the ion source microwave generator and an unexplained trip of the LH_2 target refrigerator. An expert was flown in from Toronto to repair the microwave tube, but it did not function reliably at full power for the remainder of the run, and this caused problems for the beam stability. The ion source problems were followed by a major rf spark which destroyed some high voltage components that had to be fabricated on site by the RF group, losing 5 days of beam time. Unfortunately the rf was very unstable following this repair, and this too had a major effect on the beam quality for the subsequent data-taking.

Despite the problems described above, a total of 260 data runs were acquired, grouped into 6 sets distinguished by the beam line helicity tune. The raw data obtained during May-June, 1999 are shown in Fig. 4; the raw statistical error is 0.4×10^{-7} but the poor chisquared indicates, as in the past, that significant corrections will have to be made for systematic errors. Data analysis is currently under way. This is more challenging than earlier data sets because of intermittent periods of noisy data with poorly constrained energy modulation from the ion source. A very preliminary result for the May-June, 1999 data set is $(0.7 \pm 0.4) \times 10^{-7}$.

Summary and outlook

Major progress on data acquisition and analysis has been made during the past year, resulting in an improved understanding of the sensitivity to intrinsic polarization moments and their effect on the A_z data. An analysis technique has been developed to minimize the uncertainty in this correction procedure, but this relies on achieving optimal cyclotron and beam tune conditions over extended periods of time, as experienced in the benchmark February, 1997 data set.

Preliminary analysis has already indicated that the existing full parity data set should be accurate at the $\pm 0.3 \times 10^{-7}$ level, including corrections for all

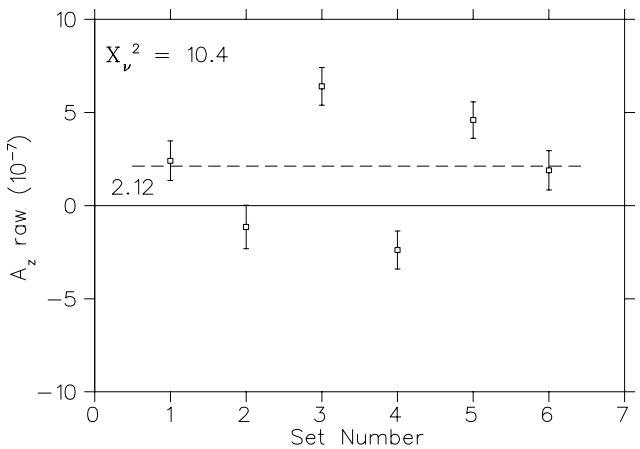

Fig. 4. Raw analyzing power data for the May-June, 1999 run.

measurable systematic effects. Analysis is ongoing to determine the best upper limit on the systematic error due to beam energy modulation, which is inferred from control measurements interleaved with parity data-taking, as discussed in earlier reports.

The preliminary result from the combined February, 1997 and July, 1998 data is shown in Fig. 5, together with recent theoretical predictions. Also shown are the highest precision existing experimental data in this energy range. The TRIUMF data point supports the meson exchange prediction at the level of this first result. Note that the uncertainty is limited by statistics, with the raw statistical error and the statistical uncertainty associated with the measurement of polarization moments (the dominant systematic error) being of comparable value. Because A_z at 221 MeV is so close to zero, reducing the *fractional* error in A_z to the level of the experiment at 45 MeV shown in Fig. 5 would require a factor of 9 more data with the existing apparatus. The collaboration has hence decided to publish a result based on the data taken so far and to investigate the possibility of mounting a new measurement with improved apparatus.

The final result from Expt. 497 will serve to determine uniquely for the first time an experimental constraint on the weak meson nucleon coupling constant h_ρ^{pp}. Already the preliminary TRIUMF result supports the DDH best value prediction for h_ρ^{pp}.

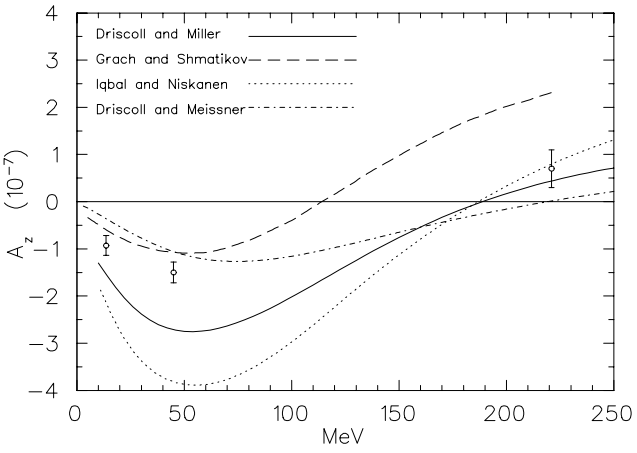

Fig. 5. Theoretical predictions for A_z in pp scattering, calculated [Driscoll and Miller, Phys. Rev. **C39**, 1951 (1989); *ibid.* **C40**, 2159 (1989)] using DDH predictions for the weak meson-nucleon coupling constants; also shown are quark model calculations [Grach and Shmatikov, Phys. Lett. **B316**, 467 (1993)], meson exchange calculations [Iqbal and Niskanen, Phys. Rev. **C42**, 1872, (1990)] and a calculation by Driscoll and Meissner [Phys. Rev. **C41**, 1303 (1990)]. The highest precision existing experimental data [Eversheim *et al.*, Phys. Lett. **B256**, 11 (1991); private communication (1994); Kistryn *et al.*, Phys. Rev. Lett. **58**, 1616 (1987)] are also shown. The 221 MeV point is from the February, 1997 and July, 1998 TRIUMF data.

Conclusion

Assuming the data analysis progresses as anticipated, the data-taking phase of Expt. 497 is now complete. The accuracy of the final result will be limited by systematic error corrections, and analysis is now under way to minimize the uncertainty in these corrections. It is expected that a significant new result will be published in 2000.

Experiment 614
Precision measurement of the Michel spectrum from muon decay

(D.R. Gill, TRIUMF)

The continuing veracity of the standard model of particle physics is a challenge to the practitioners of that art. There are indications that this model is not a complete explanation of the nature of the fundamental particles and their interactions. As a consequence, physicists are stimulated to search for data that will indicate where the theory needs improvement and/or replacement. Muon decay, which has served in the past as an important laboratory for standard model physics, will be revisited shortly in several new experiments. Examples are the two Michel parameter (η, and ξ'') experiments at PSI that have both recently seen test beam. Add to this the two muon lifetime proposals for PSI and you see that Expt. 614 at TRIUMF is part of a new, large assault on the standard model using the muon laboratory. Expt. 614 at TRIUMF will measure with high precision the differential spectrum, $d^2\Gamma/dX\,d(\cos\theta)$, of positrons from the decay $\mu^+ \rightarrow e^+\nu_e\overline{\nu}_\mu$ for polarized muons. This spectrum is commonly referred to as the Michel spectrum and the parameters therein are referred to as the Michel parameters of which the two mentioned above are examples. Here X is the positron energy ($X = 1$ corresponds to the maximum positron energy $E_{\max} = 52.83$ MeV), θ is the angle between the muon spin direction and the positron momentum. Significant improvement in our knowledge of the values of the Michel parameters ρ, δ and $P_\mu\xi$ is the goal of the TRIUMF experiment. Expt. 614 will employ the 100% polarized "surface" muon beam, which has a momentum of 29.8 MeV/c, from the M13 beam line at TRIUMF as the muon source.

During 1999, Expt. 614 passed several important milestones. The first of these was a review in January, by an international committee, of the Expt. 614 detector concept. This committee stated that they were satisfied that all the technical requirements were understood and made several recommendations regarding the development of the detector. The most significant suggestion was that the Expt. 614 collaboration construct a pre-production prototype (PPP) of an XY module of the detector, including the final design elec-

tronics, before embarking on full scale production. The collaboration accepted this advice from the committee and constructed as a PPP a single UV (XY rotated by 45 degrees) pair and its electronics. Some of the test results for this module are described below.

The second milestone for Expt. 614 in 1999 was an in-house TRIUMF review of the mechanical aspects of the detector support structure and magnetic shield. The concept for the latter is now complete and the steel has been ordered and will arrive in early 2000. Detailed drawings for construction of the shield are being prepared and will go out for machining bids in early 2000. The required holes in the shield for services to the superconducting solenoid and for the extraction of signal cables and gas hoses have been modelled using OPERA3D in order to assure that these holes do not adversely affect the uniformity of the field. The solenoid magnet will be mounted in this shield in the summer of 2000 and then the field will be mapped. The detector support structure design was changed significantly following the review, both to provide for a simpler construction and consequently to reduce construction costs. Final design drawings for the detector cradle and the track on which this cradle rides will be made early in 2000, once the magnet shield drawings are complete.

Pre-production prototype testing

The most important milestone for Expt. 614 in 1999 was the successful construction and testing of a PPP detector module, as suggested by the detector review committee. This PPP was exposed to a large series of tests during the construction phase and as a detector following its completion. Some of these construction phase tests were continuations of tests already undertaken. For example, the aluminized mylar foils that serve as cathode planes in the detector are being examined for their ability, once stretched, to maintain a minimum tension. To determine what the initial tension must be, several foils have been stretched to a variety of initial tensions and their relaxation with time has been followed. Figure 6 shows the results for a cathode foil that has now been followed for 300 days. One surprise from these tests is the long time scale over which these foils relax, in this case with a mean life of 84 days. The other test foils show similar results, relaxing at about the same rate to about 75% of the tension to which they were originally stretched. The final tension of the foil shown in Fig. 6 is adequate for the Expt. 614 drift chambers.

The first choice gas for the Expt. 614 drift chambers is dimethyl ether (DME) since the electron drift has a very small Lorentz angle. This means that corrections to the drift distances will be small if this gas can be employed. However, DME is a very "aggressive" gas;

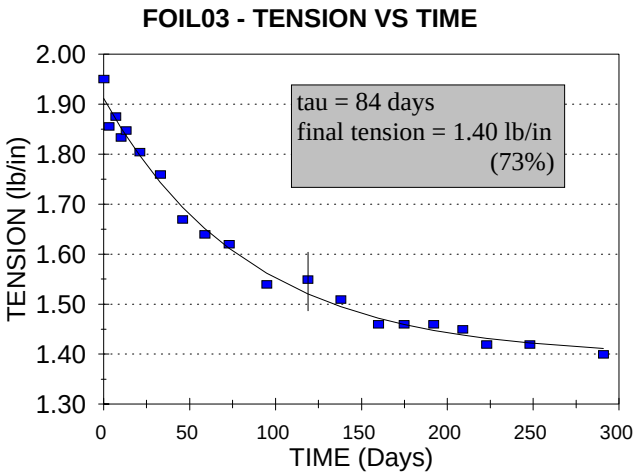

Fig. 6. Cathode foil relaxation versus time.

many things dissolve in it. The proposed materials for the Expt. 614 chambers have therefore been tested to determine whether they are attacked by DME. There are two ways that susceptible materials can influence the detector: the structural integrity and "aging". The latter refers to the fact that materials, when deposited on the wires of the detectors, degrade the signals from those wires. The weakening of materials that are exposed to DME is determined by visual examination and by mechanical testing. The test for aging effects is conducted by flowing DME past a sample of the material in question and then passing this gas through a single wire chamber that is exposed to a high level of irradiation over a short length of this wire. The lower frame in Fig. 7 shows the result of such a test for a material that results in severe aging of the irradiated region of the chamber. This material (urethane) is not acceptable for any part of the detector where it could be exposed to DME. The upper frame in Fig. 7 on the other hand shows minimum aging for an accumulated charge far in excess of that to which the Expt. 614 detector will be exposed in the lifetime of the experiment. This material, the activated copper and molecular sieve of the gas filtering system, is therefore acceptable for use in purifying the DME gas.

During the assembly of the PPP module all detector assembly procedures and their corresponding quality control (QC) techniques were exercised. All of the aspects of the assembly being QCed and most of the QC techniques were found to perform as required. An example is the tensioning of the wires and the procedure for testing that tension. Figure 8 presents the results of QC measurements of the tension achieved in one plane. In this figure the upper frame shows the results versus wire number, the outer wires on each end being for the larger diameter shield wires that were deliberately tensioned higher. The uniformity of the

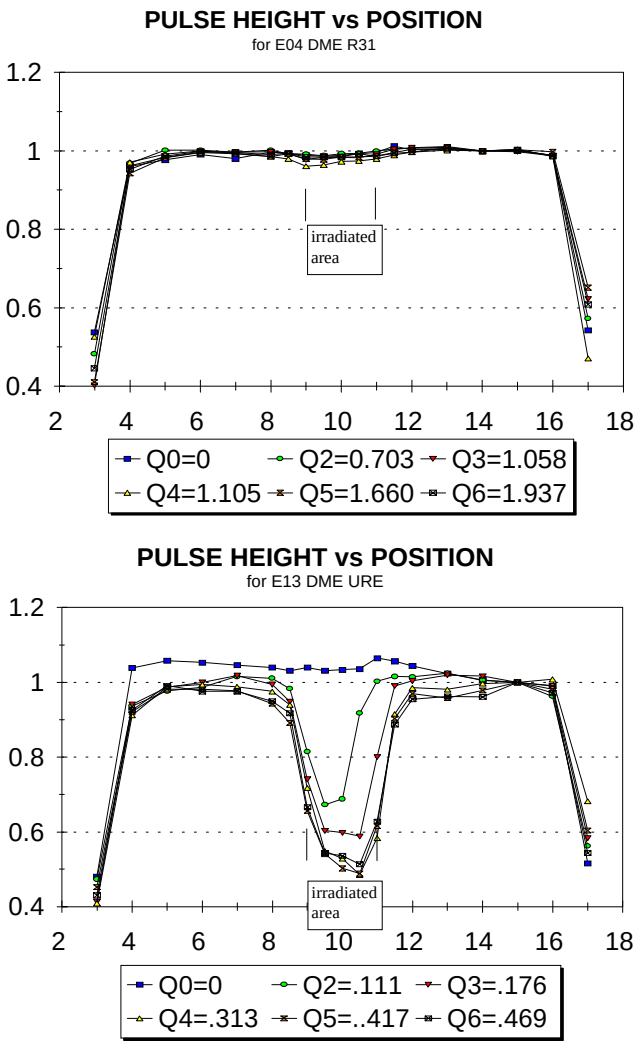

Fig. 7. Aging of a wire chamber due to materials exposed to DME.

signal wire tensions across the plane is very good as is shown in the lower frame where the σ is of order 1 g. Modifications are under way on those procedures that were judged to have performed marginally, for example the wire positioning QC and logging system. While the wires were positioned very accurately, as required, and the QC measuring system was able to demonstrate this, the latter did not function without repeated calibrations. The platform of this QC/logging system is therefore being replaced with a more accurately manufactured one to eliminate this problem.

Once the assembly was complete the performance of the PPP module as a drift chamber was examined. These tests included such studies as a scan across the detector with sources to study the pulse height response. The detector and the electronics performed as required. A major test of detector performance was done using protons from BL2C. The original beam schedule called for the employment of M11 for these

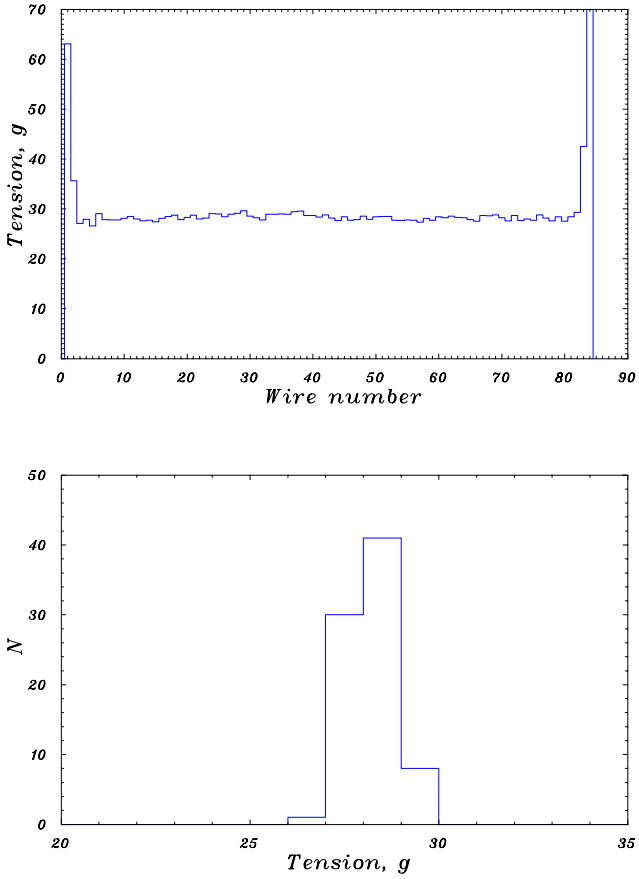

Fig. 8. Anode wire tension, top – versus wire number, bottom – distribution.

tests, but due to BL1A problems beam there was not available. The construction of the PPP had to be accomplished on a very tight schedule in order to achieve this test before the beam went off for the fall shutdown. Meeting the date of this milestone showed that the time estimates for construction of the entire Expt. 614 detector are reasonable. BL2C protons of 37 MeV were used to emulate the passage of surface muons (4 MeV) through the detector. The signal from these highly ionizing particles is very large compared to that from the minimum ionizing 52 MeV/c positrons from muon decay. The detector, however, must be operated for highest possible sensitivity for these positrons so the signals from the passing muons may produce significant crosstalk problems. Figure 9 shows the crosstalk as determined with the protons degraded to 30 MeV to simulate muons that have begun slowing down in the Expt. 614 detector array. The upper frames are TDC width information for events where only one TDC contained information. The lower frames show the same information for events where more than one TDC contained "hits". The peaks in these figures at $\approx$ channel 160 are for real hits, longer pulse duration. The peaks at $\approx$ channel 38 (short time duration = short time over threshold) in the lower frames are the contents

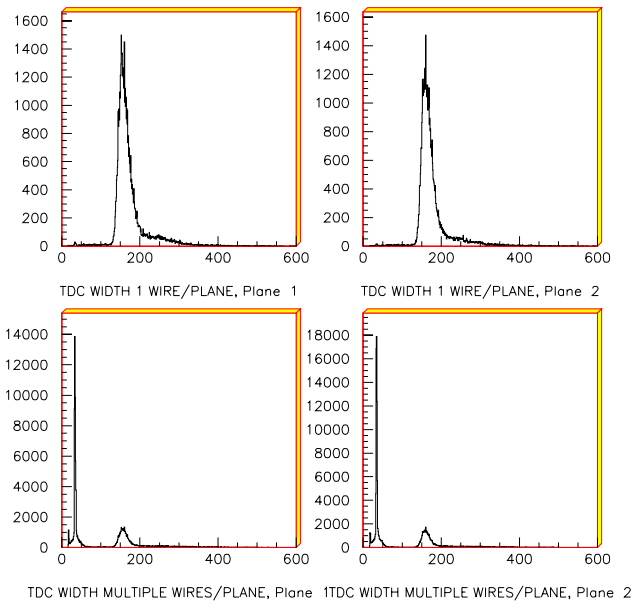

Fig. 9. Width of hit and crosstalk pulses as recorded by the TDCs.

of channels neighbouring those with the real hits, i.e. crosstalk. From these figures it is estimated that the muons will induce crosstalk in neighbouring channels ≈41% of the time. It is also obvious from these figures that a simple cut on pulse width will be a very efficient way to eliminate this problem and make tracking of the muons practical.

While the accuracy of the tracking of the muons is not of great importance to the success of Expt. 614, the tracking of the weakly ionizing positrons will be fundamental. Minimizing the crosstalk between wires for positron tracks is therefore very desirable. An ^{55}Fe source was used to emulate the passage of the weakly ionizing positrons. The crosstalk between channels was found to be non-uniform across the wire planes. The crosstalk was ≈2.5% between most of the wires while it was less than 1% for some others. It was determined that this result was due to the routing of the leads from the wires to the pre-amplifiers; those with small crosstalk were well separated while those with larger crosstalk were crowded. This crowding was determined to be unnecessary, it evolved primarily for making of convenient connections. Once this crowding was reduced, by making more judicial use of the space available, crosstalk levels were found to be ≤0.8% for all wires. This level of crosstalk is excellent for the purposes of Expt. 614.

These beam and source tests of the PPP also served as tests of the post-amp/discriminators (PD) and the data acquisition (DAQ) system. The PD and the DAQ both functioned as required. The PDs are housed in CAMAC crates and a control/monitoring unit will be installed in each crate. These units are now being designed. Analog information is required from the proportional chambers near the Expt. 614 stopping target. The electronics units for this purpose are presently being designed.

With all the test results from the PPP now indicating that the detector will function as required, the Expt. 614 collaboration will embark on mass production of detector elements in early 2000. The goal will then be to install the detector array into the magnet in the fall of 2000. This will follow the mapping of the field and the alignment of the magnet with the M13 surface muon beam. Experiment 614 would then expect to take "engineering" data to be followed by initial experimental data in the first intense beam period of 2001.

Experiment 614 software development also passed a number of milestones during 1999. The GEANT based Monte Carlo program progressed to the point where version 1.0 was released for use by the collaboration; in fact by year end the version number had advanced to 1.2. The analysis software, now based in F90, has also progressed significantly during 1999 with the version number now at 2.0. These software packages are compatible with use on several platforms. This development work will continue in 2000 with the goal of being ready for real data in late 2000.

Experiment 705
Experiment to detect ΛΛ hypernuclei using microstrip gas chambers

(C.A. Davis, TRIUMF)

BNL Experiment 885 is a search for $S = -2$ systems, namely ΛΛ-hypernuclei, Ξ-hypernuclei, and the H particle. E885 was carried out at the D6 line of the AGS at BNL (2 GeV K beam). The beam line is characterized by an excellent $\frac{K}{\pi}$ ratio (∼2–3) and a large acceptance (0.065 sr).

Some of the E885 running time was spent with a CH_2 target to produce free Ξ^- hyperons. The Ξs left the production target, were degraded, and stopped in a scintillating fibre array (SciFi) which acted as a secondary target as well as a detector. The Ξ hyperons could then form $S = -2$ exotic systems with target nuclei. After several weeks of running, a target switch was made. The majority of the running time then utilized a chemically vapour-deposited diamond target, in which the Ξ^- hyperons were created by the kaon beam but then stopped in the higher density material to perhaps be captured to form ${}^{12}_{\Lambda\Lambda}$B or other $S = -2$ objects. As well, direct production through (K^-, K^+) on carbon is possible.

Data analysis efforts are searching for evidence of the following doubly strange species:

$$(\Xi^-,{}^{12}\mathrm{C})_{\mathrm{atom}} \rightarrow {}^{12}_{\Lambda\Lambda}\mathrm{B} + n \qquad \text{(stopped } \Xi^-\text{)}$$

$$K^- + {}^{12}\mathrm{C} \rightarrow {}^{12}_{\Lambda\Lambda}\mathrm{Be} + K^+ \qquad \text{(direct production)}$$

$$K^- + {}^{12}\mathrm{C} \rightarrow {}^{12}_{\Xi}\mathrm{Be} + K^+ \qquad \text{(direct production)}$$

$$K^- + {}^{12}\mathrm{C} \rightarrow H + K^+ + X \qquad \text{(direct production)}$$

$$(\Xi^-,{}^{12}\mathrm{C})_{\mathrm{atom}} \rightarrow H + {}^{11}\mathrm{B} \qquad \text{(stopped } \Xi^-\text{)}$$

A fuller description of the experiment and the microstrip gas chambers (MSGCs) can be found in last year's Annual Report. The MSGCs, especially the downstream pair, were placed as close as possible to the target. From this position we expected an improvement in the tracking, which would lead to better determination of the outgoing K^+ momentum and therefore of the excitation energy of the recoiling system (the presumed Ξ-hypernucleus), and improved knowledge of the production vertex in the target.

The MSGC information collected during the data-taking run of BNL E885 was incorporated in the analysis. The residuals are shown in Fig. 10. The excitation energy is presented in Fig. 11.

Analysis was also carried out in parallel at Kyoto and Carnegie Mellon. These latter efforts have resulted in two papers accepted for publication (see the Publications section of this Annual Report) in addition to our report, published in Nucl. Instrum. Methods in Phys. Res. **421**, 31 (1999), on the MSGCs.

Mr. M. Landry is completing the analysis and his thesis at present and is expected to be finished by the end of 1999.

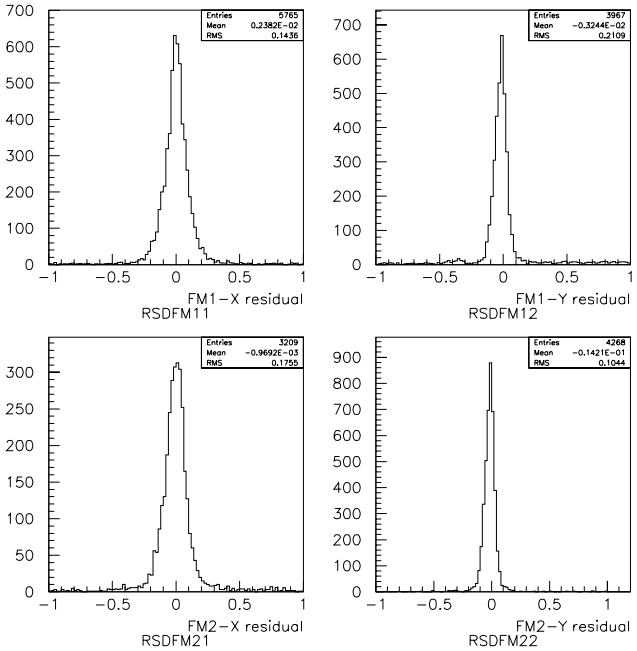

Fig. 10. Microstrip chamber residuals, measured in centimetres, for carbon data.

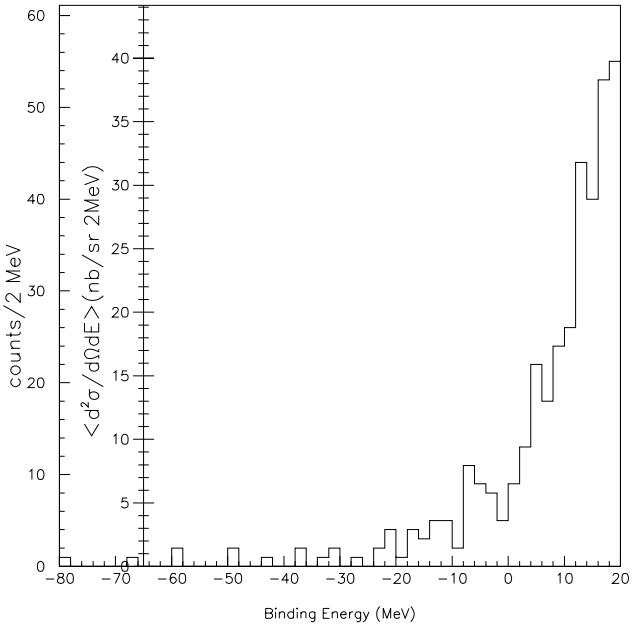

Fig. 11. Excitation energy spectrum for the diamond target with MSGC information included.

Experiment 761
Measurement of parity violation in $p-p$ scattering at 450 MeV
(J. Birchall, S.A. Page, W.T.H. van Oers, Manitoba)

The 221 MeV parity experiment at TRIUMF will isolate the weak ρ meson-nucleon coupling constant. A further experiment at 450 MeV (Expt. 761) will provide a different constraint on weak coupling constants by measuring a roughly equal combination of the weak ρ and ω coupling constants. A precise measurement at 450 MeV taken with the 221 MeV and low energy results will pin down the weak meson-nucleon coupling constants and show how (or whether) the low and intermediate energy results for the parity-violating longitudinal analyzing power, A_z, can be reconciled with the large values seen at 800 MeV and in the region of 5 GeV.

Experiment 761 was approved at high priority a few years ago by the TRIUMF Experiments Evaluation Committee. Active work on the experiment, however, had to await completion of experimental running on the 221 MeV experiment. Now that the end is in sight, an NSERC grant for R&D funding for Expt. 761 has been applied for.

Most of the equipment used for the 221 MeV measurement will also be suitable, with minor modification, at 450 MeV. In some ways the 450 MeV measurement will be easier than that at 221 MeV: multiple scattering will be less and beam size smaller, thereby decreasing sensitivity to beam size modulation; there will be lower sensitivity to beam energy modulation;

polarimeters will benefit from higher analyzing power and scattering cross section.

The following points are being considered in preparation for a 450 MeV experiment. Some are not specific to a 450 MeV experiment, but upgrades to the existing set-up.

- An update of the data acquisition system.
- Optimizing beam dynamics.
- Greatly improved polarization profile monitors.
- Possible improvements to the ionization chambers.
- Possible digitization of ion chamber signals before taking the signal difference.
- Upgrades of the liquid hydrogen target.
- Even better performance from the polarized ion source.

The ATLAS experiment at the LHC

(C. Oram, TRIUMF)

As described in detail in the 1996 Annual Report, ATLAS is building a general purpose *pp* detector which is designed to exploit the full discovery potential of the Large Hadron Collider (LHC) at CERN. The TRIUMF group is responsible for the engineering of the hadronic endcap (HEC) calorimeter, and the feedthroughs for the endcap cryostat. For the HEC, this year has seen the continuation of module production and the beginning of the design of the wheel assembly equipment, while for the feedthrough project, at the University of Victoria, the group has placed its major materials orders and in early 2000 will start production. The TRIUMF HEC group has this year started close collaboration with a Chinese group. This group is a three university cluster of Nanjing University, USTC Hefei, and Shangdong University.

Physics goals

The present theoretical understanding of elementary particles is in the context of the standard model. The standard model is a remarkably successful model, providing predictions which have been consistently confirmed by experiment for over two decades. Its agreement with experimental results, to enormous accuracy in some cases, makes it the most accurately verified model in science. Of the many elementary particles contained in the standard model, only the Higgs remains to be discovered. The central goal of ATLAS is the search for the Higgs particle.

There are good theoretical reasons to believe that the discovery of the Higgs will at least contain hints at, and more likely direct evidence of, what lies beyond the standard model. If the Higgs is composite, its existence requires as yet unknown ultra-strong forces. If it is elementary, it would be the only spinless particle to be discovered so far. There is a theoretical 'naturalness' problem for the masses of spinless particles. In the standard model, which is a highly nonlinear dynamical system, the elementary particles tend to take on the heaviest of all possible mass scales which in such a model are at inaccessible energies and inconsistent with other requirements of the model. All other particles discovered thus far have natural mechanisms, such as gauge and chiral symmetries, for protecting their masses so that they can lie in the observable range. For the Higgs particle, there is no such symmetry in the present model. The only theoretical scenarios which leave the Higgs particle light enough to observe are hypothetical ones, either technicolour or supersymmetry, both radical departures from the present structure of the standard model. If Higgs is seen at LHC, one of these scenarios should be seen at the same time.

Particle theory has progressed enormously over the last few decades with many appealing scenarios for physics beyond the standard model. The most likely of these is supersymmetry and the boldest of these is superstring theory. These theories are intimately related and are both radical ideas which promise a new conceptual framework for understanding elementary particles. Though far from being complete theories so far, there are superstring models which resemble the standard model in their low energy limit. These models have a great appeal as they contain a unification of fundamental forces which includes gravity. They have already had substantial impact on gravitational physics where, for example, in addition to the long sought reconciliation of gravity with quantum mechanics, they have been used to derive a fundamental understanding of black hole thermodynamics. Superstring theory is still in its infancy, but progress has been dramatic and the promise of great things to come has captured the imagination of a substantial fraction of the world's theoretical particle physicists.

The present theoretical view is that the conventional grand unification of the strong, weak and electromagnetic forces can only work in the supersymmetric extension of the standard model. In that model, the grand unified energy scale is only two decades below the Planck scale, the ultimate energy where spacetime itself has quantum fluctuations. It is not out of the realm of imagination that, at energy scales where supersymmetry would be observed, evidence for an ultimate theory of everything, at least everything that can exist once spacetime is formed, is within human grasp.

Experiments at LHC, where the ATLAS detector will take data, will probe the energy region where the Higgs particle, possibly supersymmetry, or other structures will be visible. This will be the first experimental probe of an energy region where fundamentally new

physics is expected to occur in many years. There is every reason to believe that the results will be among the most dramatic ever.

Basic ATLAS design considerations

The most prominent issue for the LHC is the quest for the origin of the spontaneous symmetry-breaking mechanism in the electroweak sector of the standard model (SM). This is related to one of the most fundamental questions of physics: What is the origin of the different particle masses? New direct experimental insight is required to answer this question.

One of the possible manifestations of the spontaneous symmetry-breaking mechanism could be the existence of a SM Higgs boson (H), or of a family of Higgs particles ($H^{\pm}$, h, H and A) when considering the minimal supersymmetric extension of the standard model (MSSM). The Higgs search is therefore used as a first benchmark for the detector optimization. For the SM Higgs, the detector has to be sensitive to the following processes ($\ell = e$ or μ) in order to cover the full mass range above the expected discovery limit of LEP of about $m_H > 90$ GeV:

$H \to b\bar{b}$ from WH, ZH and $t\bar{t}H$ using a $\ell^{\pm}$ and b-tagging,
mass range $80 < m_H < 100$ GeV;

$H \to \gamma\gamma$
mass range $90 < m_H < 150$ GeV;

$H \to WW^* \to \ell^{\pm}\nu\ell^{\pm}\nu$
mass range $150 < m_H < 200$ GeV;

$H \to ZZ^* \to 4\ell^{\pm}$
mass range 130 GeV $< m_H < 2m_Z$;

$H \to ZZ \to 4\ell^{\pm}, 2l^{\pm} + 2\nu$
mass range $m_H > 2m_Z$;

$H \to WW, ZZ \to l^{\pm}\nu + 2$ jets, $2\ell^{\pm} + 2$ jets
from WW, ZZ fusion using tagging of forward jets for m_H up to about 1 TeV.

Here the inclusion in the above list of the decay of the Higgs to WW^* has significantly improved the sensitivity to the Higgs in the energy region around twice the mass of the Z. The sensitivity of ATLAS to the standard model Higgs is displayed in Fig. 12. The sensitivity improvement can be seen by comparing with the same figure in the 1998 TRIUMF Annual Report.

In addition to signatures similar to these, the MSSM Higgs searches also require sensitivity to processes such as:

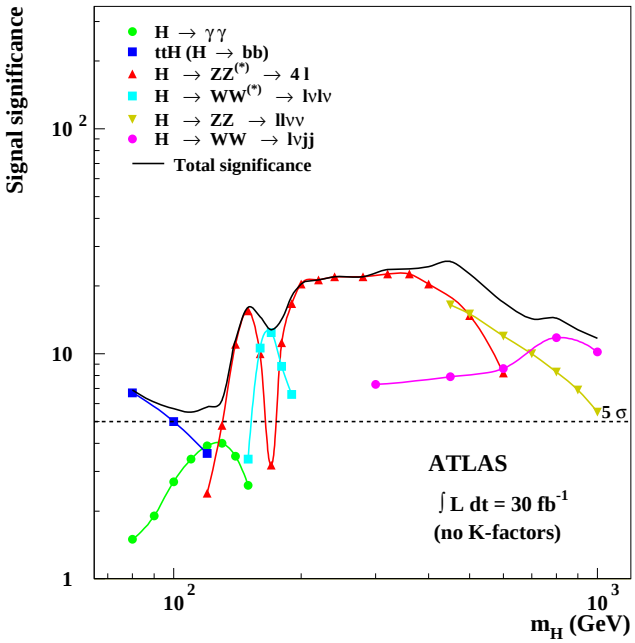

Fig. 12. Expected significance in ATLAS of the standard model Higgs boson signal, as a function of the Higgs mass, for an integrated luminosity of $10^5 \mathrm{pb}^{-1}$ for several decay channels.

$A \to \tau^+\tau^-$ $\to e\mu + \nu$'s
$\to \ell^{\pm}$ + hadrons + ν's;
$H^{\pm}$ $\to \tau^{\pm}\nu$ from $t\bar{t}$ $\to H^{\pm}W^{\mp}b\bar{b}$ and using $\ell^{\pm}$ tag and b-tagging.
$\to$ 2 jets.

The observable cross sections for most of these processes are small over a large part of the mass range to be explored at the LHC. Hence it is important to operate at high luminosity, and to maximize the detectable rates above backgrounds by high-resolution measurements of electrons, photons, and muons.

Canada's participation in ATLAS

The Canadian group consists of 35 grant eligible physicists from TRIUMF, University of Alberta, Carleton University, CRPP, UBC, University of Toronto, University of Victoria, and York University. We are strongly involved in three construction projects centred around detecting hadrons in the endcap region: the hadronic endcap project, the hadronic portion of the forward calorimeter project, and the pipeline electronics for calorimetry. In addition we are committed, as part of our common project contribution, to providing the feedthroughs for the two endcap cryostats. This project is described in detail in the ATLAS section of the Accelerator Technology Division chapter of this Annual Report. TRIUMF is directly involved in all these projects, and in the trigger and physics simulations.

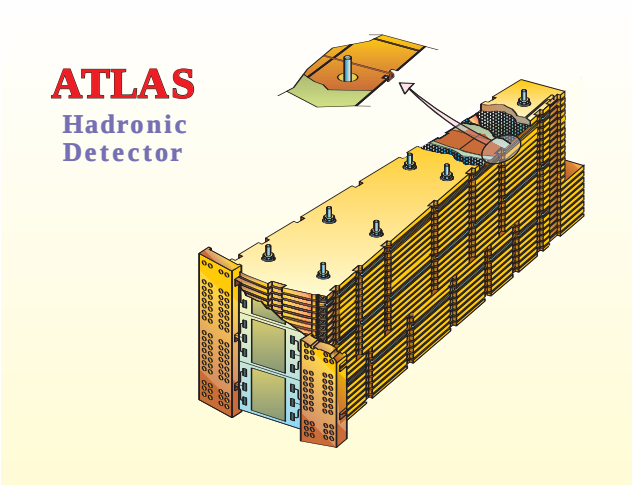

Fig. 13. Artist's impression of a hadronic endcap module.

The hadronic endcap project

The hadronic endcap calorimeter (HEC) is a liquid argon sampling calorimeter with copper absorbers [ATLAS Collab., ATLAS Liquid Argon Technical Design Report (1996)]. A concise overview of this design was provided in the TRIUMF 1996 Annual Report. An artist's impression of a module can be seen in Fig. 13.

Hadronic endcap module production

Last year the major milestone of successfully passing the Production Readiness Review process at CERN allowed us to enter into series module production this year. This was interrupted when some readout foils, manufactured in Russia, developed shorts in the test beam at CERN in the spring. This was found to be due to the materials being used not having the anticipated thermal expansion coefficient. A careful design review was undertaken and the design was modified to allow for a wider range of expansion coefficient. During this time component production such as readout board and copper plate production at TRIUMF and the University of Alberta has been proceeding at or ahead of schedule. Once the new design of the boards has passed test beam, a new manufacturing stage will start where we catch up with module stacking.

Test beam measurements of the hadronic endcap modules

Two test beam periods on the CERN H6 beam line this year have tested the performance of the production modules of the calorimeter. The H6 beam line provides beams from 20 to 180 GeV. The set-up was improved to allow for 6 rather than 4 modules in the beam. This new set-up provides superior shower containment. Analysis of the data is on-going, and provisional results show the anticipated performance. The layout of the beam line and associated systems is described in detail in the 1998 TRIUMF Annual Report.

Preparations for wheel assembly at CERN

32 modules of the HEC form a wheel. There are two wheels at each end of ATLAS, so we must construct 128 modules into 4 wheels. The equipment to undertake this is a Canadian responsibility. The engineering is being undertaken by a collaboration between CRPP and TRIUMF personnel. The preliminary design review took place this year in the fall at Marseille (CPPM). The successful completion of that review has allowed the project to enter the detailed design stage.

The BaBar experiment at the Stanford Linear Accelerator Center

(C. Hearty, UBC)

Introduction

1999 has been an exciting year for BaBar, one for which the Canadian group has been preparing for several years (Fig. 14). The group, together with American and Italian colleagues, constructed the BaBar drift chamber at TRIUMF, making extensive use of the TRIUMF infrastructure. Last year was spent commissioning the chamber and preparing for data-taking by writing reconstruction, on-line and analysis software. This work has led to the completion of the detector and the start of the first physics run. Both BaBar and the accelerator, PEP-II, performed well during the initial data-taking. As is described below, the drift chamber has met its design performance goals.

The goal of BaBar is to study CP violation in the decay of B^0 mesons at the Stanford Linear Accelerator Center. The origin of CP violation is one of the most important unresolved issues in particle physics, as it is an essential ingredient to our understanding of the baryon-antibaryon asymmetry in the universe. The only experimental observation of CP violation is in K^0 decays. The standard model describes these observations using an imaginary phase in the CKM matrix, but it is not known whether this explanation is correct.

The study of B^0 decays to CP eigenstates promises a definitive test of the standard model of CP violation. More generally, it will provide us with a series of unique consistency tests of the quark sector of the standard model and the best opportunity for precision determination of CKM parameters.

Status of the PEP-II e^+e^- collider

PEP-II is a high-luminosity storage ring that collides 9 GeV electrons with 3.1 GeV positrons. In approximately 20% of annihilations, an $\Upsilon(4S)$ is produced, moving at approximately half the speed of light in the laboratory.

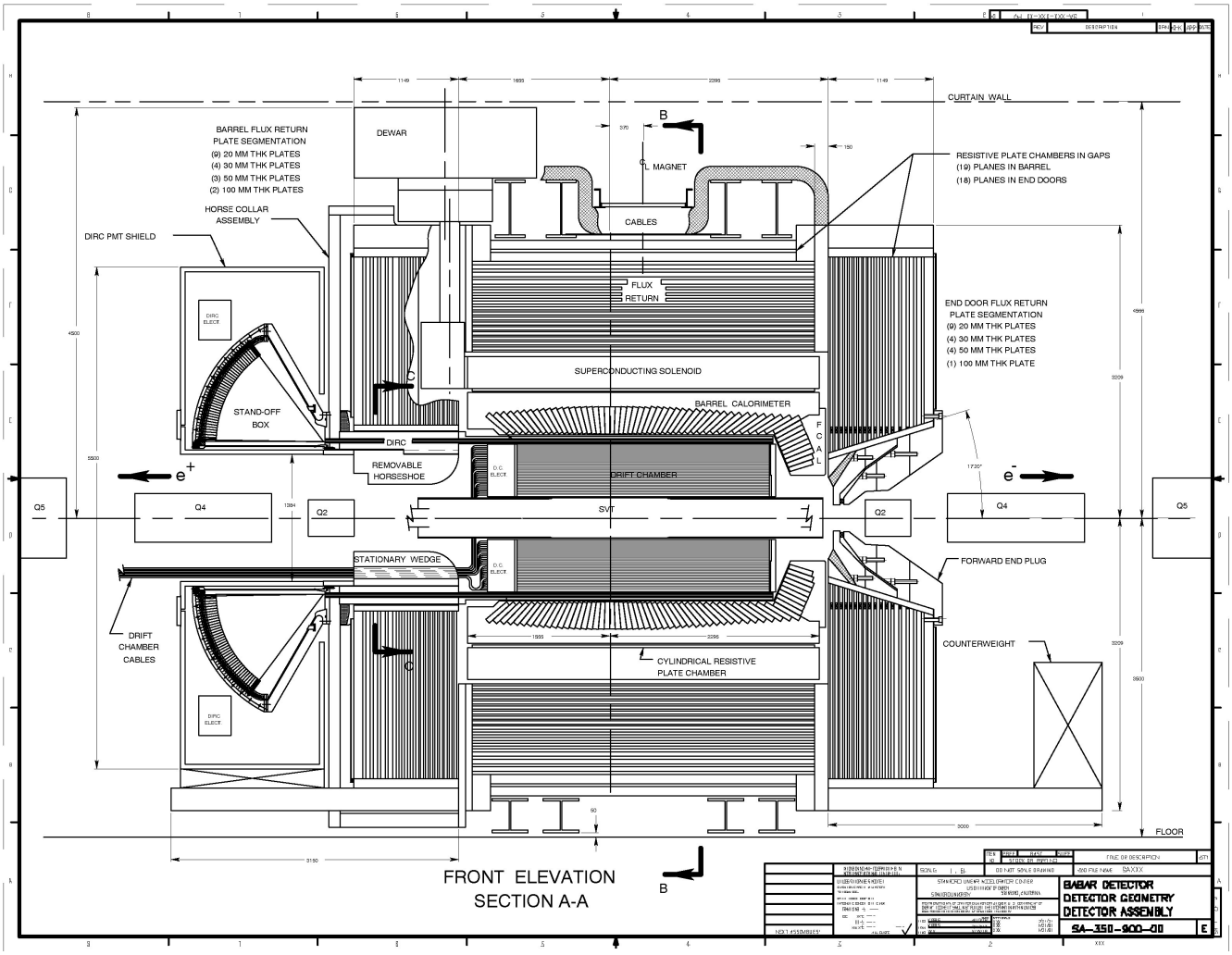

Fig. 14. The BaBar detector.

The $\Upsilon(4S)$ decays 50% to B^+B^- and 50% to $B^0\overline{B^0}$. The two B mesons are almost at rest in the $\Upsilon(4S)$ frame, with no additional particles, but the boost of the centre of mass ensures that the two decays are separated in the laboratory. This is an ideal situation for the complete reconstruction of rare decay modes.

Shortly after first collisions were recorded by BaBar on May 26, the centre of mass energy was scanned to ensure that the accelerator was operating at the peak of the $\Upsilon(4S)$ resonance. The results confirmed the PEP-II energy scale (Fig. 15).

PEP-II has rapidly increased in luminosity and efficiency since the first collisions. A peak luminosity of 1.4×10^{33} has been achieved, approximately 40% of design. BaBar has an efficiency of 90% for recording this data, leading to a total integrated luminosity of 1.7 fb^{-1}, of which 0.2 fb^{-1} was recorded at an energy below the threshold for producing $B\overline{B}$ pairs.

Backgrounds have been low enough to have no significant impact on reconstruction. At typical beam

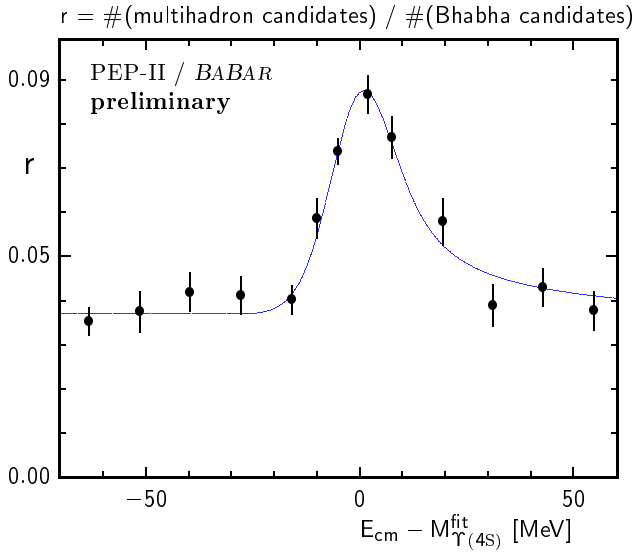

Fig. 15. The $\Upsilon(4S)$ resonance was scanned to confirm the PEP-II energy scale.

currents of 0.6 A of electrons and 1.0 A of positrons, the random occupancy in the drift chamber is 1–2%, well below the target of 10%. The design currents are 0.75 A and 2.15 A respectively.

The lost beam particles that are responsible for the backgrounds can also produce radiation damage in BaBar, particularly in the silicon vertex tracker (SVT). The allowable lifetime dose for the SVT is estimated to be 2–5 Mrad. So far, the maximum integrated dose – for the inner-most modules in the horizontal plane – is 0.1 Mrad, well within the specified target of 0.24 Mrad/year. To protect against high doses, pin diodes mounted on the detector dump the PEP-II beams when instantaneous dose rates are high. The experiment is optimizing the tradeoff between efficient operation and detector lifetime.

BaBar detector performance

The BaBar detector was completed and commissioned in 1999. The final component of BaBar to be installed was the quartz radiator bars of the DIRC particle identification system in October, part way through the first run. The DIRC is a unique device, which uses Ĉerenkov radiation to distinguish charged pions from kaons and other particles. The power of the DIRC is illustrated in Fig. 16, which shows a significant enhancement in the reconstruction of D^0 mesons through the decay to $K^+\pi^-$. The efficiency for identifying kaons in this channel is 80% within the acceptance of the DIRC.

The most critical detector component for physics analysis is the tracking system, which consists of the

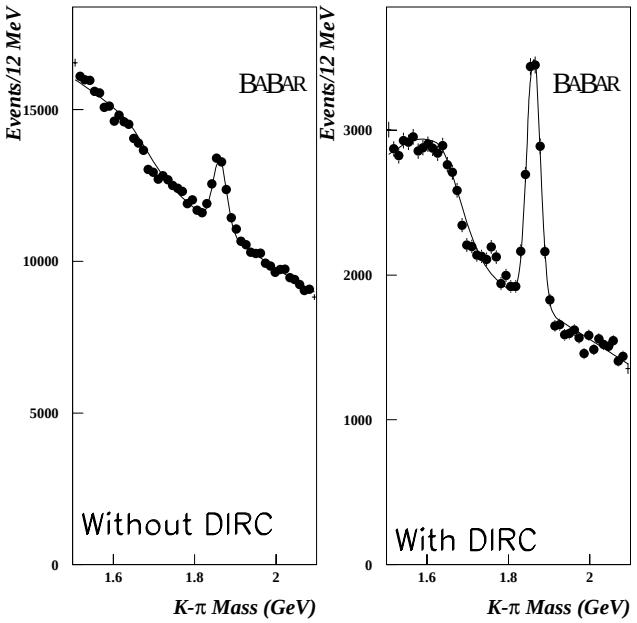

Fig. 16. D^0 candidates reconstructed via the $K^+\pi^-$ decay mode without and with the DIRC.

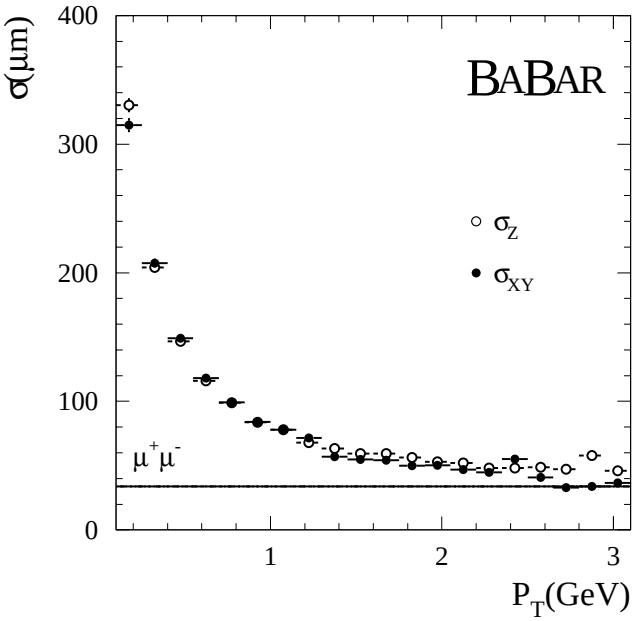

Fig. 17. The resolution on the distance of closest approach of a track to the primary vertex for hadronic events and dimuons.

SVT and the drift chamber. The ability to locate the origin of each track is essential in reconstructing the two B mesons in each event. Figure 17 shows the resolution per track on the distance of closest approach of the track to its origin. The resolution is adequate to cleanly separate the two primary B vertices, which are separated by an average of 270 μm. The other primary figure of merit is the momentum resolution. BaBar has achieved a resolution for high-momentum tracks ($p_t > 3.5$ GeV/c) of $\sigma_{p_t}/p_t = 0.3\% \cdot p_t$, the design value. Improvements may be possible with further study of the alignment between the drift chamber and the SVT and within the drift chamber itself.

The drift chamber can assist the DIRC in identifying charged tracks by using the energy deposited per unit length in the chamber gas, dE/dx (Fig. 18). The chamber alone will provide $\geq 3\sigma$ separation between pions and kaons up to momenta of 700 MeV/c.

BaBar analysis

The first stage in the analysis of BaBar data is the reconstruction of signals recorded in the detector components into physics-related quantities, such as energy and momentum. As of the end of 1999, a total of 2×10^8 events have been processed using a farm of 100 SUN computers. A batch farm of an additional 70 SUNs provides users with access to the data, which are stored in an object-oriented database, called Objectivity. BaBar is developing a non-Objectivity storage method for the subset of data needed for most physics analysis so that this data can be distributed to other analysis sites. One such site is being set up at the University of Victoria.

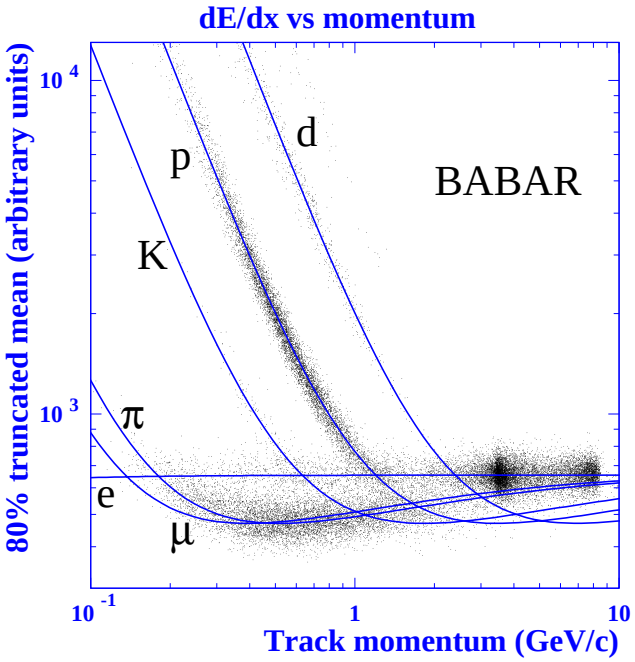

Fig. 18. Energy deposited per unit length in the drift chamber gas as a function of momentum for different particle species.

Work is under way on producing physics tools, such as particle identification software, and on physics analyses that demonstrate the ability of the BaBar hardware and software to produce quality physics results.

An area of physics tools in which the Canadian group has a large responsibility is the development of muon identification software. Muons are identified by the absence of electromagnetic or hadronic showering, and their penetration through material. The flux return of the solenoid, a total thickness of 60 to 65 cm of iron, is instrumented with resistive plate chambers for this purpose.

Inclusive D^{*+} reconstruction

One demonstration analysis is the reconstruction of D^{*+} mesons via their decay to $D^0\pi^+$, where $D^0 \to K^-\pi^+$. The kaon and pion are kinematically fit to a common vertex to form the D^0, which is then combined with the low-momentum π^+ to obtain the decay vertex of the D^{*+}. A plot of the difference in mass of the $K^-\pi^+\pi^+$ and the $K^-\pi^+$ shows a clear peak near 145 MeV/c^2, equal to the mass difference of the D^{*+} and the D^0 (Fig. 19).

Reconstruction of $B^+ \to J/\psi K^+$

The decay $B^+ \to J/\psi K^+$ is the charged B meson equivalent of the CP violating decay $B^0 \to J/\psi K_s$. No CP violation should be observed in this final state, so it can be used as a control sample for the kinematically similar B^0 decay. J/ψ candidates are formed from oppositely-charged tracks from a common vertex. Both

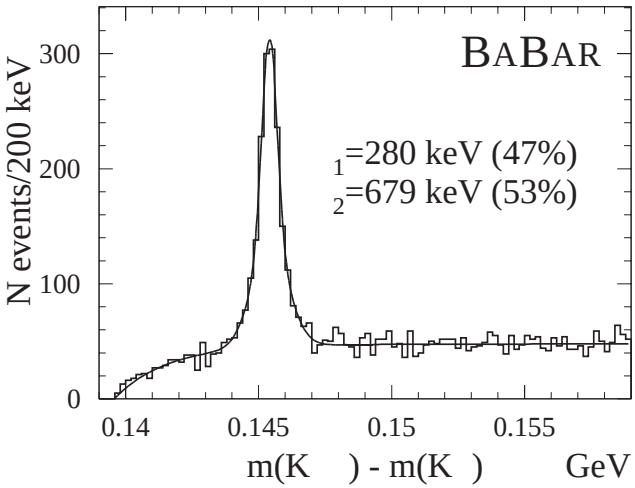

Fig. 19. Mass difference between $K\pi$ and $K\pi\pi$ candidates. The peak is located at the mass difference between the D^0 and D^{*+} mesons.

particles must be identified as electrons or muons, and the mass of the pair must be close to the expected value. The J/ψ is combined with a K^+ candidate (any track) to form a B^+ candidate, including constraints of the J/ψ and K^+ masses, a common vertex, and the beam energy.

Two analysis variables are then used to select actual B^+ events: ΔE, the difference between the energy of the B^+ candidate and the beam energy prior to the beam energy constraint, and m_B, the mass of the candidate after the application of the beam energy constraint. Figure 20, which is based on 620 pb^{-1} of data, shows a clear accumulation of 19 events at the expected values. The estimated background is 1.82 events. Figure 21 shows the mass distribution for events passing the ΔE cut.

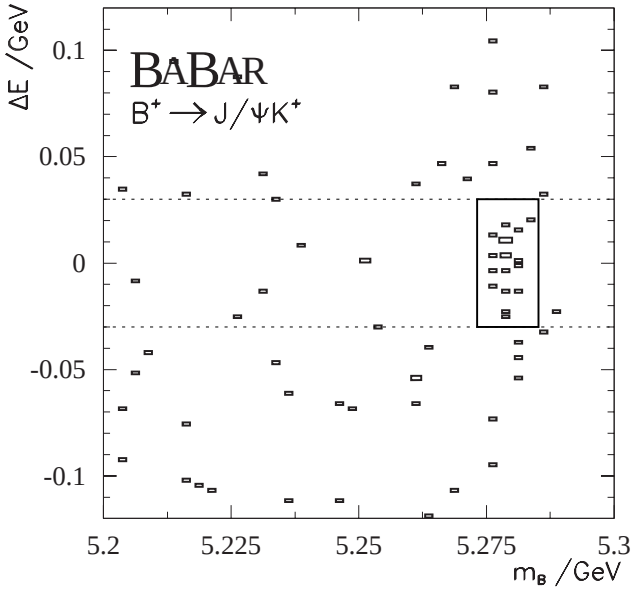

Fig. 20. Scatter plot of the two kinematic analysis variables used to identify B^+ candidates.

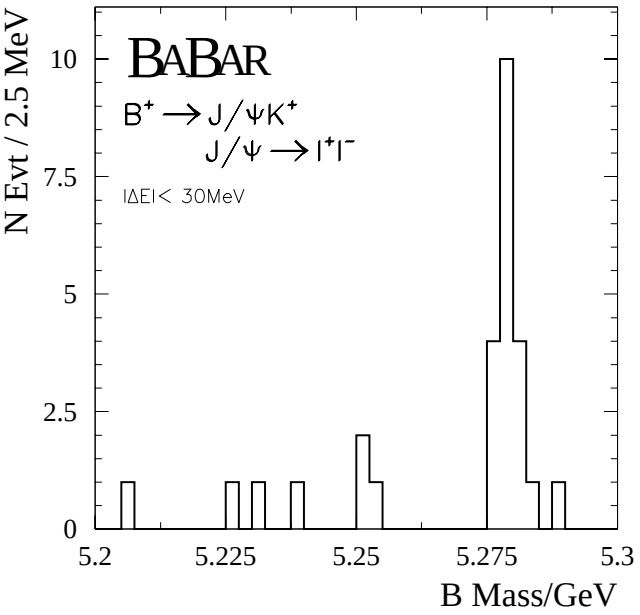

Fig. 21. Reconstructed masses of the B^+ candidates reconstructed via the $J/\psi K^+$ final states.

Outlook

The CP violating mode $B^0 \to J/\psi K_s$ is considered to be the "gold-plated" method of measuring $\sin(2\beta)$. The analysis is similar, except that the candidate K^+ is replaced by a candidate K_s, which is formed from a pair of oppositely charged tracks coming from a common vertex. The rate for this final state is approximately 30% of the $J/\psi K^+$ rate.

An initial measurement of CP violation should be possible for a data sample of approximately 10 fb^{-1}. BaBar looks forward to collecting a sample of at least this size during the 10 month run scheduled for 2000.

BNL 787
Study of rare K decays

(D. Bryman, TRIUMF/Victoria/UBC)

Unique opportunities to elucidate the details of quark mixing and the origin of charge-parity (CP) non-invariance are presented by the rare kaon decays $K^+ \to \pi^+ \nu\bar{\nu}$ and $K_L \to \pi^0 \nu\bar{\nu}$.

In the standard model (SM) calculation of $B(K^+ \to \pi^+ \nu\bar{\nu})$, the dominant effects of the top quark in second order weak loops make this flavour-changing neutral current decay very sensitive to V_{td}, the coupling of the top to down quarks in the Cabibbo-Kobyashi-Maskawa quark mixing matrix. A fit based on the current phenomenology gives a prediction of $(0.82 \pm 0.32) \times 10^{-10}$ for this branching ratio [Buchalla and Buras, Nucl. Phys. **B548**, 309 (1999)]. If constraints from $|V_{ub}/V_{cb}|$ and ϵ_K are not imposed, a limit $B(K^+ \to \pi^+ \nu\bar{\nu}) < 1.67 \times 10^{-10}$ can be extracted that is almost entirely free of theoretical uncertainties.

In 1997 BNL 787 published evidence for the decay $K^+ \to \pi^+ \nu\bar{\nu}$ [Adler *et al.*, Phys. Rev. Lett. **79**, 2204 (1997)] based on the observation of a single event from the 1995 run at the Brookhaven AGS. The branching ratio determined from that analysis was $(4.2^{+9.7}_{-3.5} \times 10^{-10})$. Although consistent with the standard model expectation, the central experimental value exceeds it by a factor of four and the possibility of a larger-than-expected branching ratio [Nir and Worah, Phys. Lett. **B423**, 319 (1998)] has sparked increased interest in the results from more sensitve measurements using the complete BNL 787 data set obtained from subsequent AGS running periods. In 1999 the analysis effort was focused on the 1996-97 data set including an improved re-analysis of the 1995 data which yielded the published event.

The goal was to reduce the total expected background to significantly less than one event in the combined data. The search for $K^+ \to \pi^+ \nu\bar{\nu}$ events was restricted to the limited background region with measured momentum $211 < P_{\pi^+} < 229$ MeV/c, between the $K_{\mu 2}$ and $K_{\pi 2}$ peaks. Compared to the published analysis, improvements in the kinematic reconstruction routines were made to reduce the tails of the momentum, range and energy resolution functions. In the new analysis, the position of the incident kaon at the last beam counter was used to refine the correct kaon-stopping position in the target, and thus to reduce the uncertainty in the pion range masked by the kaon track. Accidental hits that might have been included in the pion energy measurements were identified and removed more efficiently. The axial component analysis of the pion track in the range stack was optimized by using the most reliable information from the drift chamber fit and the end-to-end timing in the range stack scintillators. In addition, improvements were made in the particle identification criteria based on measurements of the $\pi \to \mu \to e$ decay sequence.

The new signal selection and background rejection criteria resulted in roughly halving the expected backgrounds per kaon decay, and in increasing the acceptance by 23% to $A = 0.0021 \pm 0.0001^{\rm stat} \pm 0.0002^{\rm syst}$. The 10% systematic uncertainty is based, for example, on tests made with the known branching ratios of $K_{\mu 2}$ and $K_{\pi 2}$ decays. Analysis of the full data set yielded only the single event previously reported from which the branching ratio is $B(K^+ \to \pi^+ \nu\overline{\nu}) = 1.5^{+3.3}_{-1.2} \times 10^{-10}$. This result is being prepared for publication in early 2000.

Analysis efforts are now engaged with the final BNL 787 data set taken in 1998 with a sensitivity roughly comparable to that of the previous total 1995-97 data. The study of this ultra-rare decay will continue as BNL 949 after the detector undergoes upgrades designed to

achieve a sensitivity of $\sim 10^{-11}$, a factor of 5–10 below the SM prediction.

HERMES

Nucleon spin structure and studies of QCD

(M.C. Vetterli, TRIUMF/SFU; C.A. Miller, TRIUMF/Alberta)

The main focus of the HERMES experiment is the study of the spin structure of the nucleon using the deep inelastic scattering (DIS) of 27.5 GeV polarized positrons/electrons from polarized internal gas targets ($\vec{\mathrm{H}}, \vec{\mathrm{D}}, {}^3\vec{\mathrm{He}}$) in the HERA storage ring. In addition, much thicker unpolarized targets have been used in a rich program of studies of various aspects of QCD.

The main advantages of HERMES are the purity of its targets (no dilution of the observed asymmetry) and the relatively large acceptance of the spectrometer, which allows hadrons to be detected in coincidence with the scattered positrons. For polarized target studies, this leads to the determination of the contribution to the nucleon spin from each individual quark flavour, and perhaps also from the gluons. Unpolarized targets have been used to study the hadronization of the quark as it leaves the nucleon and medium modifications to structure functions and hadronization.

Some physics topics that were of particular interest this year are discussed in the following sections: specifically, the polarized quark distribution functions ($\Delta q(x)$), the contribution to the nucleon spin from the gluons, the measurement of a single-spin azimuthal asymmetry, and the first observation of a dependence on nuclear mass of the ratio R of longitudinal to transverse DIS cross sections. The running conditions for 1999 as well as the status of the Canadian contributions to the experiment will be presented first.

The 1999 HERA run

HERA delivered beam in two periods in 1999. All polarized target data were taken with deuterium.

January–April:

Good data collection started in late February after repetitive difficulties with beam polarization. The experimental conditions were then very good, resulting in about 10^6 DIS events being collected. A small target cell (19.0 cm × 8.0 cm vs. 29.1 cm × 9.8 cm) was tested at the beginning of this period. The target thickness was expected to double due to the reduced conductance of the smaller cell. Unfortunately, it was not possible to determine its polarization performance because the electron beam was dumped into the cell wall in the first week of the run, resulting in low target polarization. A standard cell was used for the rest of the period.

Mid June–mid December:

This period started with a test of the transverse target configuration. It was confirmed that the effect of the transverse holding field on the beam could be compensated and that heating from increased synchrotron radiation was negligible. Furthermore, the background rates in the spectrometer were found to be acceptable. This test was done in anticipation of the transverse target program to be done after the HERA luminosity upgrade. The longitudinal target chamber was reinstalled in July and data were recorded in this configuration for the rest of the year. Problems with beam polarization and with the incompatibility of running conditions at ZEUS and HERA-B led to poor data collection in August and part of September. However, conditions steadily improved and were very good in November and December. Approximately 1.2×10^6 DIS events were collected during this period. In addition to the $\vec{\mathrm{D}}$ target, a Kr target was used in a 3-day dedicated run to extend to a heavier nucleus studies of medium modifications of R and of hadron attenuation in semi-inclusive scattering as a function of nuclear radius. Finally, at the end of this period, a medium sized target cell (21.0 cm × 8.9 cm) was installed. This cell has worked beautifully with high polarization, high atomic fraction, and almost twice the thickness of the old target.

The Canadian hardware contribution

The Canadian group's (Alberta, Simon Fraser, and TRIUMF) main contribution to HERMES hardware was the transition radiation detector (TRD) and its associated gas system. The TRD exceeds its performance goal (100:1 pion rejection factor at 90% positron efficiency) and continues to work without major problems. Particle identification algorithms continue to be improved and HERMES enjoys better sample purity than expected. A. Miller is leading the effort to produce a forward quadrupole spectrometer (FQS) consisting of small drift chambers installed inside the first accelerator quadrupoles downstream of the HERMES spectrometer. The FQS will measure positrons scattered at very small angles, which go down the beam pipe and are deflected in the quadrupoles. This will extend the measurement of the kinematics of the scattered positron down to very small negative four-momentum transfer Q^2. Four of these detectors are now working *in situ*.

Physics results

Polarized quark distributions

As outlined in last year's Annual Report, the main thrust of the HERMES physics program is the determination of the spin distribution of individual quark

flavours in the nucleon using semi-inclusive DIS measurements. The basic idea is called flavour tagging, and relies on the fact that a hadron of a given type detected in the final state has different probabilities of originating from quarks of different flavours. For example, a π^+ likely comes from a u quark since it is a $(u\bar{d})$ state and the u quark dominates the scattering. Contributions by the d quark are enhanced in π^- $(d\bar{u})$ production. Data on the production of various hadrons from various targets are combined in a global fit with inclusive scattering data to determine the contribution of each quark flavour to the spin of the nucleon. Preliminary results on polarized quark distribution functions were shown in last year's Annual Report. This analysis was finished in 1999 and the results were published in Physics Letters [HERMES collaboration, Phys. Lett. **B464**, 123 (1999)]. Figure 22 shows the spin dependent parton distributions for u, d, and sea quarks. The improvement over the only previous data from SMC can be seen in the top panel which shows the valence quark distributions. The contribution from sea quarks is not well determined because the semi-inclusive data set is not yet complete and the hadrons used in the current analysis were not identified. Furthermore, the inclusive data do not distinguish between quarks and anti-quarks (the coupling of the virtual photon is the same for q and $\bar{q}$). As a result, the uncertainty on the combinations $u + \bar{u}$ and $d + \bar{d}$ is smaller than on u_V and d_V. The $u + \bar{u}$ and $d + \bar{d}$ distributions are plotted in the bottom panel of Fig. 22. The precision of the polarized quark distributions as a function of x is now very good, approaching that of the unpolarized distributions, albeit over a more restricted kinematic range. It should be noted that the uncertainties on the d quark and sea distributions will be greatly reduced by including the 1999–2000 data on $\vec{D}$, which have a larger fraction of events coming from the d quark. We expect the uncertainties on the d quark distributions to be similar to those currently on the u quark.

The gluon spin distribution and high p_t hadrons

A decade of experiments have not succeeded in identifying the missing contribution to the nucleon spin, the conclusion being that only a small net fraction of the total spin comes from the quark helicities. The leading candidate to account for the missing fraction is a gluon contribution. This quantity is not simple to determine because the gluon does not couple directly to the virtual photon in leading order DIS. Processes must be found where the contribution from gluons is important, or even dominates. One such process is photon-gluon fusion (PGF) where any asymmetry depending on the relative spin direction of the beam and the target can be ascribed to a polarization of the gluons in the nucleon. For example, PGF has the largest

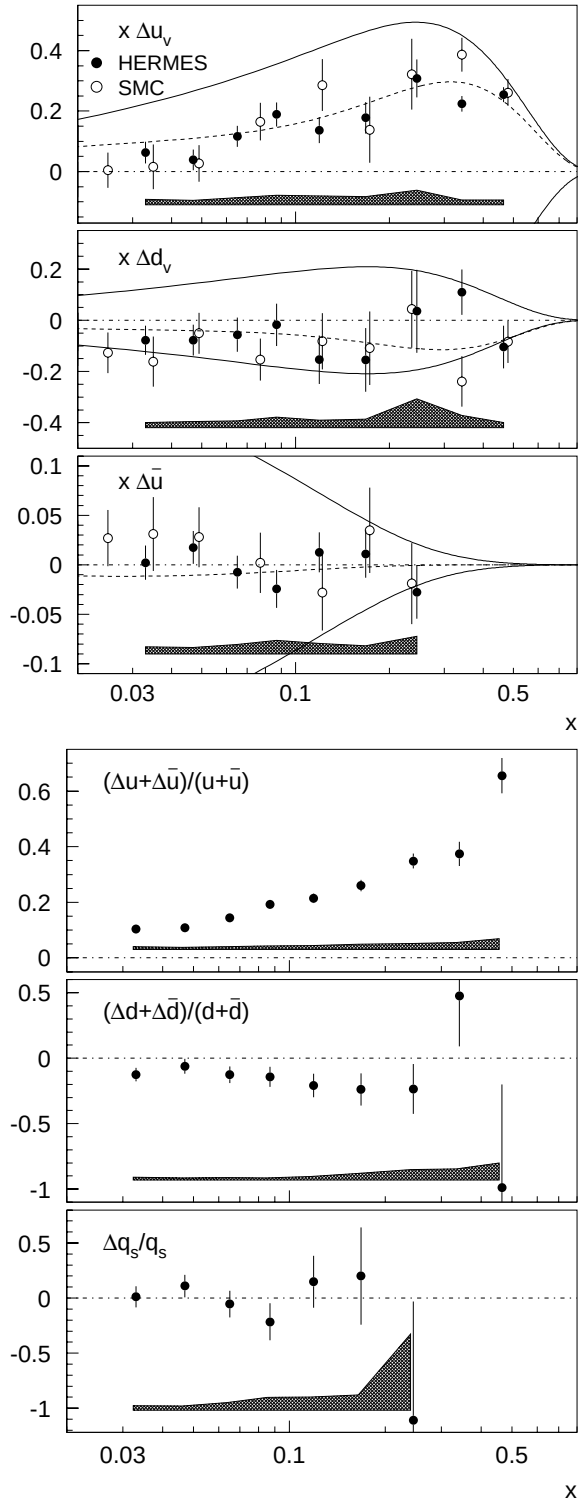

Fig. 22. (Top) Polarized valence quark distributions from HERMES at $Q^2 = 2.5$ GeV^2 (filled circles) compared to SMC (open circles). The solid lines indicate the positivity limit, while the dashed lines are a parameterization from Gehrmann and Stirling. (Bottom) Flavour decomposition of the polarized quark distributions. In both plots, the error bars for HERMES are statistical, while the bands represent the systematic uncertainty. The total uncertainties are shown for the SMC data.

contribution to the production of hadrons containing a charm quark. HERMES has done several upgrades in order to increase the sensitivity to charm production in both the J/ψ and open charm channels. Another process which is dominated by PGF is the production of pairs of oppositely charged hadrons with large transverse momentum. HERMES has observed an asymmetry in this process, which is shown in Fig. 23. The quantity:

$$A_{\parallel} = \frac{N^{\uparrow\downarrow}L^{\uparrow\uparrow} - N^{\uparrow\uparrow}L^{\uparrow\downarrow}}{N^{\uparrow\downarrow}L_P^{\uparrow\uparrow} + N^{\uparrow\uparrow}L_P^{\uparrow\downarrow}}$$

is plotted where p_t^{h1}, the transverse momentum of the hadron with the higher p_t, is greater than 1.5 GeV/c. $N^{\uparrow\downarrow}$ and $N^{\uparrow\uparrow}$ are the number of oppositely charged high-p_t hadron pairs in the two relative beam-target spin orientations. L and L_P are the dead-time corrected luminosities in the appropriate spin states, L_P being weighted with the beam and target polarizations. The curves in the figure are explained in the caption. The best fit to the data using a LO QCD model implemented in the PYTHIA Monte Carlo generator gives a gluon polarization of $\Delta G/G = 0.41 \pm 0.18 \pm 0.03$ at $\langle x_G \rangle = 0.17$. Caution should be exercised in the interpretation of the asymmetry. Other processes such as QCD Compton scattering can also lead to polarization dependent asymmetries. Furthermore, contributions from vector meson dominance diagrams or from the non-resonant $q\bar{q}$ structure of the photon could dilute any observed asymmetry. However, all models of these processes give positive (or zero) values of $A_{\parallel}$, while only photon-gluon fusion gives a negative asymmetry, as observed in the data. Any underestimate of the other contributions would therefore lead to a larger gluon polarization. These results have been accepted for publication in Physical Review Letters [HERMES collaboration, hep-ex/9907020]. The result is currently different from zero by $\approx 2.2\,\sigma$. This should be improved to 3.5–4 σ when the 1999–2000 data are included. If verified, this would be the first direct evidence of gluon polarization in the nucleon and would be a significant contribution to solving the nucleon spin puzzle.

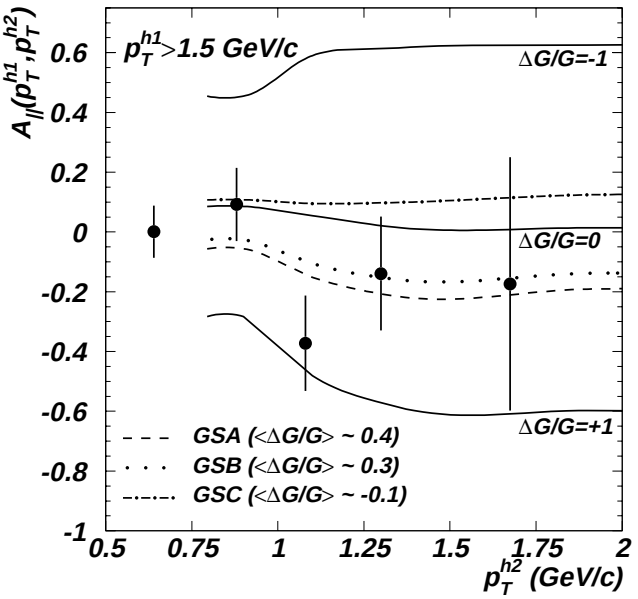

Fig. 23. The asymmetry $A_{\parallel}$ for high-p_t hadrons compared to Monte Carlo predictions for $\Delta G/G = \pm 1$ (lower/upper solid curves), $\Delta G/G = 0$ (middle solid curve), and a LO QCD fit [Gehrmann and Stirling, Phys. Rev. **D53**, 6100 (1996)].

Single spin azimuthal asymmetries

Almost all of the work done to date on polarized DIS has used a longitudinally polarized target. Transversely polarized targets can be used to study the structure function g_2, which could isolate twist-3 contributions to the scattering due to parton-parton correlations. Data on g_2 from SLAC with reasonably good precision are consistent with no twist-3 component. Transverse targets can also be used to study a third leading-twist structure function h_1. The other two are F_1 measured in unpolarized DIS and g_1 measured with a longitudinally polarized target. The function h_1 is a measure of the difference in the distributions of quark spins parallel and anti-parallel to the nucleon spin when the latter is polarized transversely to its (infinite) momentum (so-called transversity). This is similar to g_1 where the spin is, however, along the momentum of the nucleon. A comparison of h_1 and g_1 can give evidence for relativistic effects in the structure of the nucleon; h_1 and g_1 are equal in the non-relativistic quark parton model. h_1 is more difficult to measure than the other two functions because it is chiral-odd and hence cannot be measured in inclusive scattering. However, it can be measured in semi-inclusive scattering where the combination of a chiral-odd structure function and a chiral-odd fragmentation function allows the process to take place. HERMES is well placed to make the first measurement of h_1 thanks to its ability to make semi-inclusive measurements. This is in fact one of the main goals of the physics program after the HERA luminosity upgrade (see below). As stated above, the most promising way to measure h_1 requires a non-zero chiral-odd fragmentation function. Evidence for this has been found in a measurement of the azimuthal asymmetry in pion production on a longitudinally polarized target with an unpolarized or spin-averaged beam. The quantity:

$$A_{UL}^{\sin\phi} = \frac{\frac{L^{\uparrow}}{L_P^{\uparrow}} \sum_{i=1}^{N^{\uparrow}} \sin(\phi^{\uparrow}) - \frac{L^{\downarrow}}{L_P^{\downarrow}} \sum_{i=1}^{N^{\downarrow}} \sin(\phi^{\downarrow})}{\frac{1}{2}(N^{\uparrow} + N^{\downarrow})}$$

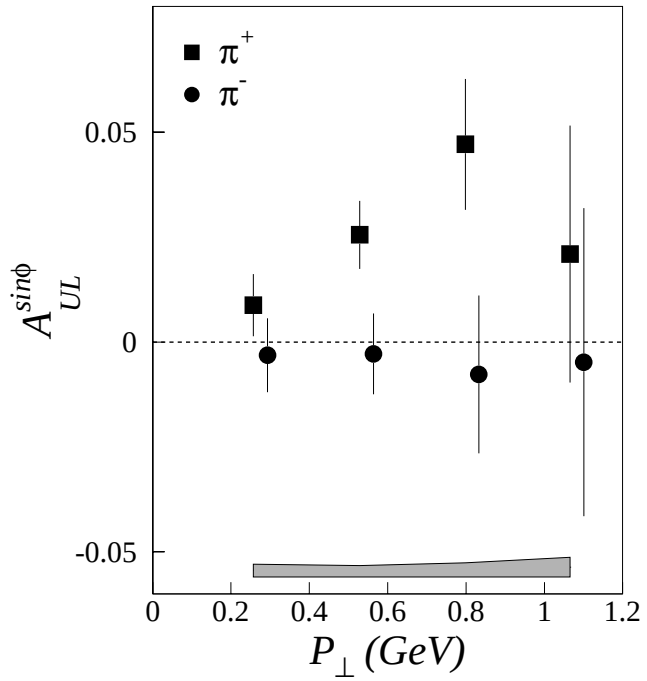

Fig. 24. Analyzing powers for the $\sin(\phi)$ moment as a function of transverse momentum for π^+ (squares) and π^- (circles). Error bars show the statistical uncertainties and the band represents the systematic uncertainties.

where the $\uparrow$ / $\downarrow$ denote positive/negative helicity of the target, is plotted in Fig. 24. Each summation is over the number $N^{\uparrow/\downarrow}$ of events involving a pion for each target spin state corresponding to the dead-time corrected luminosities $L^{\uparrow/\downarrow}$ and $L_P^{\uparrow/\downarrow}$, the latter being averaged with the magnitude of the target polarization. The clear non-zero asymmetry for the π^+ is an indication that the chiral-odd fragmentation function needed to measure h_1 is not zero, which is very promising for the transverse spin program. The smaller asymmetry for the π^- is understood in a fairly straightforward way. The asymmetry for π^+ is dominated by scattering from up quarks because the up quark is more abundant in the proton and has a higher charge than the down quark. On the other hand, the π^- asymmetry is more complicated as it receives significant contributions from both up and down quarks. These contributions probably tend to cancel because the up and down quarks can be expected to have opposite transverse polarizations, in analogy with the longitudinal case. These results have been accepted for publication in Physical Review Letters [HERMES collaboration, hep-ex/9910062].

Nuclear effects on $R = \sigma_L/\sigma_T$

The EMC collaboration discovered that the unpolarized structure function F_2^A depends on the mass A of the target. This is known as the EMC effect at intermediate values of x (> 0.1), and shadowing at low x. While the total cross section depends on A, it would be interesting to see if the transverse and longitudinal cross sections, determined by F_1 and F_L respectively, depend on A differently. Previous experiments have not extracted any dependence on A of the ratio $R = \sigma_L/\sigma_T = F_L/2xF_1$. HERMES has studied this using unpolarized ^{1}H$_2$,^{2} H$_2$,^{3} He, and ^{14}N$_2$ targets. The ratio:

$$\frac{\sigma_A}{\sigma_D} = \frac{F_2^A\,(1+\epsilon R_A)(1+R_D)}{F_2^D\,(1+R_A)(1+\epsilon R_D)}$$

where ϵ is the virtual photon polarization parameter, was measured for several targets and fits were done as a function of ϵ in several x bins to determine F_2^A/F_2^D and R_A/R_D. The results for R_A/R_D are plotted in Fig. 25. The HERMES data at lower Q^2 and x show marked deviations from unity. Furthermore, the discrepancy increases with A as one would expect for a nuclear medium dependent effect. On the other hand F_2^A was found to be consistent with F_2^D. Since F_2 and R depend differently on the longitudinal and transverse cross sections, medium effects on σ_L and σ_T can be determined separately. It is found that both an enhancement of σ_L and a reduction of σ_T are required to explain the data. This effect has generated much interest in the community. A new experiment has been approved at JLAB to verify our results, and there is much theoretical activity aimed at explaining the data. These results

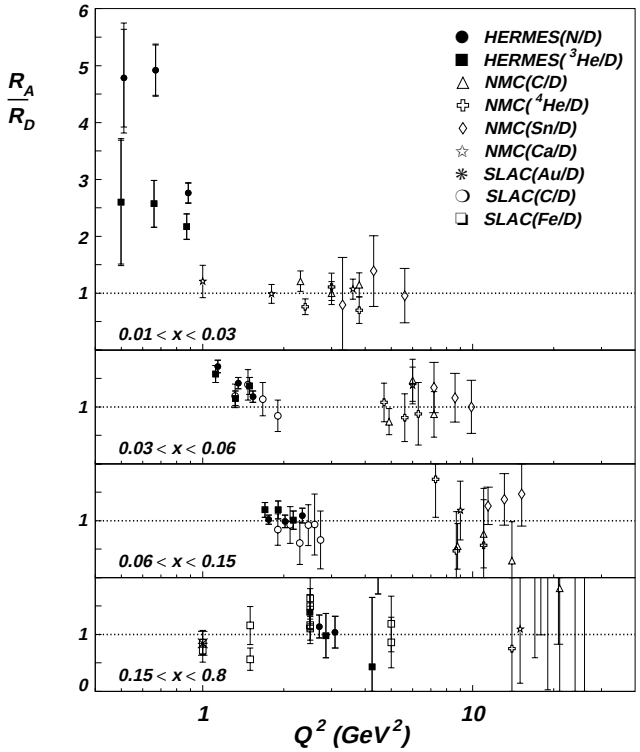

Fig. 25. The ratio R_A/R_D for nucleus A and deuterium as a function of Q^2 for four different x bins.

have been accepted for publication in Physics Letters B [HERMES collaboration, hep-ex/9910071].

Outlook

The 2000 HERA run has been extended until September at which time there will be an 8–9 month shutdown to upgrade the luminosity for the colliding beam experiments. A 25% increase in the positron beam current is planned within this program, which will also increase the luminosity at HERMES. However, it remains to be seen what effect the changes in the storage ring will have on the beam polarization. The HERMES collaboration submitted a long range plan to the HERA-PRC in the fall outlining a three-pronged physics program for the period 2001–06. This includes running with transversely and longitudinally polarized targets, as well as with unpolarized targets. The long range plan has been approved.

Transversity

As discussed above, there is much interest in measuring the third leading-twist structure function h_1, and our results on single spin azimuthal asymmetries indicate that this should be possible due to the existence of a non-zero chiral-odd transverse fragmentation function, the Collins function. This will be the focus of our start-up program after the luminosity upgrade, due to the fact that a polarized beam is not needed for these measurements. The transverse program is expected to take about two years to complete.

Improved measurements of ΔG and Δs

While the uncertainties on the polarized distributions of up and down quarks (including $\bar{u}$ and $\bar{d}$) are expected to be small by the end of the 2000 run, the strange quark distribution will not be very well determined. The measurement of the contribution to the nucleon spin by the gluons using the charm channels will also suffer from poor statistics in 2000. It is therefore planned to run for an additional two years with a longitudinally polarized target to complete these measurements.

Unpolarized targets

A rich physics program using unpolarized targets has emerged at HERMES. One aspect of this program is discussed above (A dependence of R). The advantage of unpolarized targets is that an enormous amount of data can be collected in a short period of time because the target thickness is limited only by the effect it has on the lifetime of the positron beam, and signal currents in the wire chambers in front of the spectrometer magnet. Thicknesses on the order of 10 times the polarized target thickness are possible. We will continue to take data with unpolarized targets to study topics such as the A dependence of R, hadron formation times, and tagged structure functions among others. Deeply virtual Compton scattering is an interesting new topic since it measures the total angular momentum contribution from quarks and gluons separately. When combined with previous measurements of $\Delta\Sigma$, the contribution from quark spins alone, these data might give evidence for an orbital angular momentum contribution to the nucleon spin. The studies using unpolarized targets are expected to add about one year to the HERMES program.

In closing, there is no lack of good physics for HERMES to address beyond the luminosity upgrade and the Canadian group intends to continue its involvement through this period.

People involved in HERMES include (from Alberta) staff: P. Green, L.G. Greeniaus, P. Kitching, M. Vincter, Postdoc: B. Seitz, students: L. De Nardo, G. Kotik; (from TRIUMF) staff: C.A. Miller, M.C. Vetterli, S. Yen, Postdocs/Research Associates: L. Felawka (HERMES Software Coordinator), M. Hartig, J. Ouyang, J. Stewart (HERMES Technical Coordinator); (from SFU) student: J. Wendland. We also receive technical help from H. Coombes (Alberta) and R. Openshaw (TRIUMF).

KEK Expt. 246 (Japan-Russia-Canada-Korea-U.S.A. Collaboration)

Search for T violation in $K_{\mu 3}$ decay

(M.D. Hasinoff, UBC; J.A. Macdonald, B. Shin, TRIUMF)

Violation of time-reversal invariance can be inferred from a weak interaction induced transverse polarization (P_T) of muons normal to the decay plane in $K^+ \to \pi^0\mu^+\nu_\mu$ ($K^+_{\mu 3}$) decay. Standard model (SM) contributions to P_T are around the 10^{-7} level and consequently a measurement in excess of this has the potential to reveal new CP violation physics, given CPT invariance. The motivation to search for additional sources of CP violation arises from the observed baryon asymmetry in the universe, which cannot be explained by the CP violation in the standard model alone such as the SM T violation recently observed in the neutral kaon system [CPLEAR collaboration, Phys. Lett. **B444**, 43 (1998)]. Recent theoretical progress in electroweak baryogenesis suggests that new CP violation sources might exist at the electroweak scale which can be accessible experimentally. At the High Energy Accelerator Research Organization (KEK) in Japan, the KEK 246 collaboration from Canada, Japan, Korea, Russia and the U.S.A. is conducting a search for P_T at the $\sim 10^{-3}$ level.

In 1999, a new result for P_T was obtained and published [Abe *et. al.*, Phys. Rev. Lett. **83**, 4253 (1999)],

based on ≈3.9 $\times 10^6$ good $K^+_{\mu 3}$ events from the data taken during 1996 and 1997.

KEK 246 uses stopped K^+ in contrast to the previous experiment at BNL [Blatt *et al.*, Phys. Rev. **D27**, 1056 (1983)] which used in-flight decay. The decay products are emitted isotropically and detected in a 12-sector superconducting toroidal spectrometer magnet (Fig. 26a,b). P_T is measured as the azimuthal (ϕ) polarization of μ^+ emitted radially (r) when a π^0 is tagged in the forward (fwd) or the backward (bwd) direction relative to the detector (z) axis. The signature of non-zero P_T is an asymmetry between clockwise (cw) and counter-clockwise (ccw) Michel e^+ (Fig. 26c). Summation over the twelve sectors plays an important role in reducing the systematic errors. For finite P_T, events from fwd and bwd π^0s have opposite asymmetries. By taking their difference, the P_T signal is doubled and most of the systematic errors are reduced. The sum, $fwd + bwd$, provides a sensitive null check of the apparatus.

A separated K^+ beam ($\pi^+/K^+ \approx 6$) of 660 MeV/c was produced at the 12 GeV proton synchrotron with a typical intensity of 3.0×10^5 per 0.6 s spill duration with 3 s repetition. Kaons were identified in a Čerenkov counter and degraded so as to stop in a target array at the centre of the detector. A $K^+_{\mu 3}$ event was identified by analyzing the μ^+ with the spectrometer and detecting the π^0 with a CsI(Tl) photon detector. In the CsI(Tl) barrel, there were twelve holes for muons to pass into the magnet, plus the beam entrance and exit holes. In order to maximize sensitivity, a π^0 was identified as either two photons (2γ) with invariant mass ($M_{\gamma\gamma}$), or as one photon (1γ) with an energy greater than 70 MeV which sufficiently preserved the directional information of the parent π^0. Charged particles from the target were tracked by multiwire proportional chambers at the entrance (C2) and exit (C3 and C4) of each magnet gap, along with the target array. The momentum resolution ($\sigma_p = 2.6$ MeV/c at 205 MeV/c) was adequate to remove the predominant background of $K^+ \to \pi^+\pi^0$ ($K_{\pi 2}$) decay.

Muons entering the polarimeter were degraded and then stopped in a stack of pure Al plates where the spin depolarization due to multiple scattering or relaxation was negligible. Pairs of shim plates were used to create a highly symmetric magnetic field with an average strength of 130 G at the muon stopper in order to preserve P_T, while the in-plane components were precessed. Positron counter arrays were located between the muon stoppers and the time spectra of e^+ were recorded by multi-stop TDCs up to 20 μs. Background associated with the beam was suppressed by veto counters surrounding the beam region.

Two independent off-line analyses were performed. They provided a consistency check and estimation of systematic errors associated with the analysis. The major differences between the two analyses were in charged-particle tracking, in the clustering algorithm in the CsI(Tl) array, in rejection of kaon-decay-in-flight events, and in positron detection background suppression.

Figure 27 shows the positron time spectrum (sum of 2γ and 1γ). The spectrum has a functional form $N_0 \exp(-t/\tau_\mu) + B_0$ for $t > 600$ ns with the muon lifetime of $\tau_\mu = 2.197$ μs. The signal was extracted with highest sensitivity by integrating the time spectrum from 20 ns to 6.0 μs after subtraction of the background, B_0, deduced from fitting between 6.0 μs to 19.5 μs with reduced χ^2s of 0.9 to 1.2. The flatness of

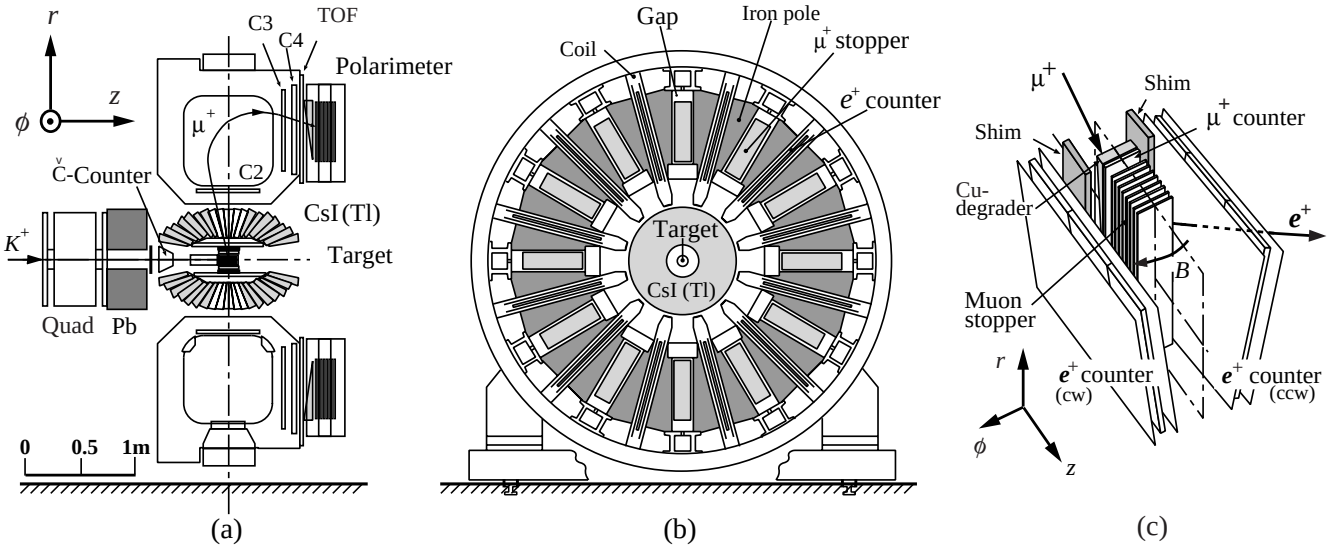

Fig. 26. Experimental set-up: (a) cross section side view, (b) end view, (c) schematic view of one sector of the polarimeter.

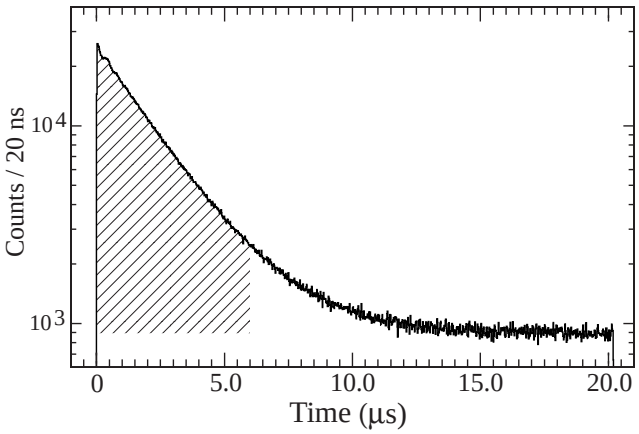

Fig. 27. Positron time spectrum of all good events (sum of 2γ and 1γ). The hatched region is the analyzed signal region after subtraction of the constant background deduced from fitting in the region from 6.0 to 19.5 μs.

the background was tested by observing the spectra of sectors not containing the event.

After null asymmetry checks confirmed that there was no significant spurious asymmetry, the T violating asymmetry A_T was extracted using a double ratio as

$$A_T = \frac{1}{4}\left[\frac{(N_{cw}/N_{ccw})_{fwd}}{(N_{cw}/N_{ccw})_{bwd}} - 1\right].$$

Here the fwd and bwd regions of π^0 (2γ) or photon (1γ) were defined by their polar angle $\theta_{\pi^0(\gamma)}$ with $|\cos\theta_{\pi^0(\gamma)}| > 0.342$ at a maximum sensitivity. This double ratio is insensitive to the systematic error coming from fwd/bwd event number difference.

The transverse polarization was computed as

$$P_T = A_T/(\alpha\langle\cos\theta_T\rangle),$$

where the analyzing power, α, was determined from the in-plane component $P_N(\perp \boldsymbol{p}_\mu)$ by comparing it with a Monte Carlo calculation. The factor α included the effects of intrinsic muon decay asymmetry, muon spin precession around the field not uniformly parallel to the polarimeter axis, positron interactions, and the finite counter solid angle. The average angular attenuation factor $\langle\cos\theta_T\rangle$ was defined for the angle θ_T of the decay-plane normal vector relative to the ϕ-axis in the polarimeter. It was evaluated by a Monte Carlo calculation which took into account the accidental background in the CsI(Tl).

The major systematic errors in P_T come from admixtures of the in-plane polarization components of $P_L(\|\boldsymbol{p}_\mu)$ and P_N. Most such admixtures are cancelled out by the 12-fold rotational symmetry of the detector as well as by the fwd/bwd ratio. The main sources were the misalignment of the detector elements, the asymmetry of the magnetic field at the polarimeter, and an asymmetric K^+ stopping distribution. Whenever possible, the cancellation power of the fwd/bwd double ratio was estimated by using real data. The spurious effects of π^+ and K^+ decay in flight were estimated from the upper bound of A_T in the background region, and from the small tilt of the incident beam, respectively. The error due to the analysis ambiguity could be estimated from the discrepancy of $\langle\cos\theta_T\rangle$ between the two analyses. The total systematic error was evaluated by adding all contributions in quadrature to be 0.9×10^{-3}, well below the statistical error.

We obtained a combined result from the two analyses of $P_T = -0.0042 \pm 0.0049(stat) \pm 0.0009(syst)$. The T violating parameter Imξ was then extracted as Im$\xi = -0.013 \pm 0.016(stat) \pm 0.003(syst)$. There is no evidence for any T violation. The 90% confidence limits are given as $|P_T| < 0.011$ and $|\mathrm{Im}\xi| < 0.033$.

Anticipation of reducing the statistical error further comes from additional data taken in 1998 and 1999, now in analysis, and with further running time scheduled for 2000.

Data for several other interesting reaction studies have also been obtained. These include the analysis of the $K^+ \to \pi^0\mu^+\nu_\mu$ decay spectrum to determine the structure functions $f^\pm$, and of $K^+ \to \pi^0 e^+\nu_\mu$ and a study of the dominant normal component of the muon polarization, P_N, in $K^+_{\mu3}$ decay. The Canadian group has undertaken the analyses of non-leptonic decays of kaons, such as $K^+ \to \pi^+\pi^0\gamma$ ($K_{\pi2\gamma}$) (BR = 2.75×10^{-4}) and $K^+ \to \pi^0\pi^0\pi^+$ ($K^+_{\pi3}$) (BR = 1.73%) since such decay modes can be used as a testing ground of QCD inspired chiral perturbation theories (χPT), as well as CP violation and the $\Delta I = 1/2$ rule.

In 1999 a paper describing a kinematically complete measurement of $K^+_{\pi3}$ was accepted for publication [Shin *et al.*, European J. Phys., in press]. The matrix element of $K^+_{\pi3}$ can be expanded [Weinberg, Phys. Rev. Lett. **4**, 87 (1960)] to lowest order in s_i as:

$$|M|^2 \sim 1 + gY + hY^2 + jX + kX^2 \ldots$$

where $Y = (s_3 - s_0)/m^2_{\pi^+}$, and $X = (s_1 - s_2)/m^2_{\pi^+}$ with $s_i = (M_K - M_i)^2 - 2M_kT_i$, and $s_0 = (M_K^2 + 2M^2_{\pi^0} + M^2_{\pi^+})/3$, and $g = 0.594 \pm 0.0219$ and $h = 0.035 \pm 0.015$. In the present experiment both of the π^0s can be reconstructed; hence the values j and k can be determined for the first time. j should be zero if CP invariance holds. If CP violation is present, it should be about –3.3 times the value observed in $K^+ \to \pi^+\pi^+\pi^-$. The coefficients h and k provide information on whether the final state contains more than one isospin state, and thus they provide a test of the $\Delta I = 1/2$ rule, which states that $\Delta I = 1/2$ transitions are dominant in kaon decays. The confirmation of this rule stems from the ratio of branching ratios, $\frac{\Gamma(\pi^0\pi^0\pi^+)}{\Gamma(\pi^+\pi^+\pi^-)}$ which

proves $\Delta I = 5/2$ and $\Delta I = 7/2$ are absent but nothing about the presence of $\Delta I = 3/2$ terms, which may arise from a $\Delta I = 1/2$ strangeness-nonconserving current. In this experiment we have determined the following values: $g = 0.518 \pm 0.039$ and $k = 0.043 \pm 0.020$. Hence the quadratic term in $(s_2 - s_1)$ is small but nonzero, and the new world average value for g becomes $g = 0.587 \pm 0.019$, in excellent agreement with the value, $g = 0.582 \pm 0.021$ for the CP symmetry partner $K^- \to \pi^-\pi^0\pi^0$. Furthermore, the $\Delta I = 1/2$ rule seems to be violated since the prediction for g_{+00} is 0.43 using $g_{++-} = -0.2154 \pm 0.004$ and $g_{--+} = -0.217 \pm 0.010$.

This kinematically complete experiment also allows a nearly model independent determination to be made of both the isoscalar and isotensor $\pi - \pi$ scattering lengths free from the usual problems caused by the final state hadronic and Coulomb interactions. Our measured values lead to a value for the Weinberg parameter in nearly perfect agreement with the value $W = 0.56$ currently predicted by the Goldberger-Treiman relation. A paper describing these scattering length results is in preparation.

TJNAF Experiment E91-017
Measurement of the flavour singlet form factors of the proton
(W.T.H. van Oers, Manitoba)

The structure of the nucleon at low energies in terms of the quark and gluon degrees of freedom is not well understood. The $G0$ experiment is to measure two proton ground state matrix elements which are sensitive to point-like strange quarks and hence to the quark-antiquark sea in the proton. The matrix elements of interest are the elastic scattering vector weak neutral current charge and magnetic form factors, G_E^Z and G_M^Z, respectively. These can be extracted from a set of parity-violating electron-proton scattering measurements. If one assumes a relationship between the proton and neutron structure in that the proton and neutron differ only by the interchange of up and down quarks, i.e., isospin symmetry, the strange quark (as well as the up and down quark) contribution to the charge and magnetic form factors of the nucleon can be determined. This would result from taking appropriate linear combinations of the weak neutral form factors and their electromagnetic counterparts.

Determinations of both the charge and magnetic strange quark form factors are of fundamental interest, as they would constitute the first direct evidence of the quark sea in low energy observables. The objective of the $G0$ experiment is to determine these contributions to the proton form factors at the few per cent level. Observations at high energy suggest that the strange quarks carry about 1/2 as much momentum as up and down quarks in the sea. It is important to determine both the role of the quark sea and the relevance of strange quarks at low energy where there are voids in understanding the theory of the strong interaction (quantum chromodynamics, QCD). Even if the strange quark contributions do not amount to the level of sensitivity of the experiment, upper limit determinations at this level are as valuable as non-zero results. The matrix elements, G_E^Z and G_M^Z, are also relevant to discussions of the Ellis-Jaffe sum rule and the pion-nucleon sigma term; there is uncertainty in both of these about the strange quark contributions. The $G0$ experiment will allow the determination of the strange quark contributions to the proton charge and magnetic form factors in a much more straightforward manner than is possible with regard to the corresponding observables in the above two determinations.

In the $G0$ experiment, parity-violating longitudinal analyzing powers will be measured in electron-proton scattering in the range $0.1 \leq Q^2 \leq 1.0$ GeV^2 at both forward and backward angles. The longitudinal analyzing power is defined as

$$A_z = \frac{1}{P}\,[\sigma^+(\theta) - \sigma^-(\theta)]/[\sigma^+(\theta) + \sigma^-(\theta)]\ ,$$

with P the polarization of the incident electron beam and the $+$ and $-$ signs indicating the helicity state. Making pairs of measurements at forward and backward angles will allow the separation of G_E^Z and G_M^Z. Predicted longitudinal analyzing powers range from about (–3 to 35) $\times 10^{-6}$; it is planned to measure the longitudinal analyzing powers with statistical uncertainties of $\Delta A/A = 5\%$ and systematic uncertainties related to helicity correlated effects of $\Delta A/A \leq 2.5 \times 10^{-7}$. In the first phase of the experiment, longitudinal analyzing powers will be measured concurrently at seven values of the momentum transfer in the range $0.1 \leq Q^2 \leq 1.0$ GeV^2. With an electron beam polarization of 0.49, the time required to reach this precision in the first phase measurement will be about 700 hours. It now appears highly probable that by the time of data-taking for the $G0$ experiment, higher beam polarizations will also be available at the reduced beam pulse frequency of 31 MHz, decreasing the data-taking time by close to a factor of two. However, it must be realized that it is not the actual data-taking time that governs the length of the experiment but rather making elaborate control measurements to determine the corrections that have to be made to the measured asymmetries and to understand systematic errors. Using the result for G_M^Z at $Q^2 = 0.1$ GeV^2 from the SAMPLE experiment now being performed at the MIT-Bates Laboratory, it would be possible to separate the charge and magnetic form factors at the lowest Q^2 bin after the first phase measurement. In the second phase experiment, each

subsequent backward angle analyzing power measurement would require from 0.5 to 1 month of running time. It should be noted that the overall uncertainties quoted for the recent low-energy proton-proton parity violation experiments at PSI and the University of Bonn, obtained in the 221 MeV proton-proton parity violation experiment at TRIUMF, and quoted for the systematic uncertainties in the electron-proton parity violation experiments at MIT-Bates (SAMPLE experiment), at TJNAF (HAPPEX experiment), and at MAMI-Mainz suggest that systematic uncertainties of a few times 10^{-7} should be attainable in the $G0$ experiment. The results of the HAPPEX experiment show that there exists no barrier at Jefferson Lab to successfully perform the $G0$ experiment.

The *G*0 collaboration

The $G0$ experiment will be carried out in Hall C at TJNAF by a collaboration of scientists from Canada, France, Georgia, and the United States, with funding provided through NSERC (Canada), IN2P3 (France), and DOE/NSF (US).

The TJNAF Program Advisory Committee reconfirmed the A priority for the $G0$ experiment in January; the experiment underwent an annual Progress Review in May. The conclusions of the Progress Review Committee included a very strong endorsement of the experiment, lauded the accomplishments made, provided various suggestions regarding project management to enhance the ability to construct $G0$ with the required performance and on cost and on schedule, and made various comments on how to further improve specific responsibilities within $G0$. Design, construction, and testing of the various $G0$ instrumentation really took flight with the resolution of a contract dispute with the vendor of the superconducting magnet system in June.

Canadian contribution to the *G*0 experiment

The Canadian members of the $G0$ collaboration, based at the universities of Manitoba and Northern British Columbia, and at TRIUMF, have been asked to: (i) develop and produce specialized photomultiplier tube bases for the main detector arrays; (ii) prototype and produce the cryostat exit detector arrays for the backward angle measurements; (iii) coordinate the implementation of TJNAF-built specialized beam monitors and control apparatus, and TRIUMF-built parity-type electronics to read out these monitors on the Hall C beam line; (iv) design, build and test an automated magnetic field measuring apparatus complete with its own data acquisition system; and (v) devise a set of measurements to determine the neutron background to which the $G0$ detector system will be subjected.

This past year has seen great progress in the designing and building of many of the various components/subsystems listed above.

The *G*0 main detector array

The heart of the $G0$ detection system is a spectrometer which consists of an 8-sector toroidal magnet, with an array of scintillation detectors located at the focal surface of each sector (see Fig. 28). Due to geometry, resolution, and rate considerations, the shapes of both the prototype scintillators and their associated light-guides have become very elaborate. Since data will not be acquired in event-by-event mode in this experiment, and since the scintillator arrays are the only detectors to measure the scattered particles in the forward angle mode, the performance of these focal-plane detectors (FPD) are of critical importance. The timing and pulse shape characteristics of this system must be fine tuned at the hardware level because it will not be possible to reconstruct individual events. Furthermore, the real signal rates associated with many of the FPD segments will be quite high (1 MHz) and the photon yields may be quite large. As such, very special demands will be made on the photomultiplier tubes (PMT) and especially on their associated divider/base circuit.

Much progress has been made in the design, development, and building of the $G0$ bases at TRIUMF. In 1997, a set of prototype high-rate bases was constructed and delivered to TJNAF for tests. Based on these studies, modifications were made and a second set of prototype bases was constructed and delivered to TJNAF in early 1998. In the summer of 1998, 12 final prototype bases were constructed and delivered to TJNAF to be used in conjunction with the first set of prototype focal-plane detectors, and fabrication of the actual production bases began in earnest. With the help of summer students (funded partly through the TRIUMF Summer/Co-op Students program and partly through the $G0$ NSERC grant), the production of the electrical components for all of the production bases was completed in the late summer of 1998.

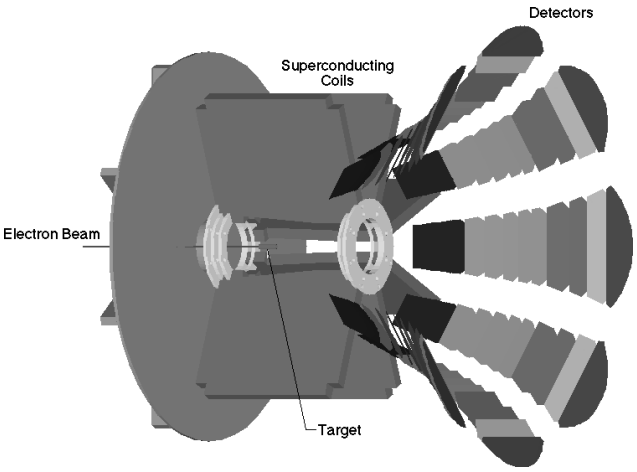

Fig. 28. View of the $G0$ superconducting toroidal spectrometer with one sector and the spectrometer housing removed.

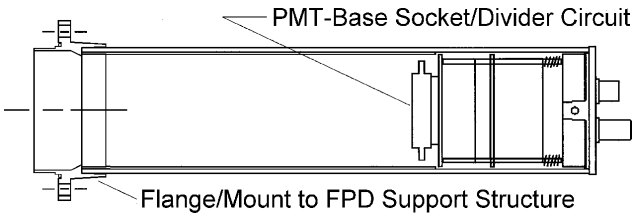

Fig. 29. Schematic layout of the TRIUMF/$G0$ PMT-base assembly.

The design of the mechanical housing for the PMT/base subsystem depended somewhat on the final design of the FPD support structure. After much effort resolving subsystem integration issues, the final design for the PMT/base housing assembly was completed in late 1998 (see Fig. 29) and procurement of parts commenced. The remaining task for this subsystem, fabrication and assembly of the mechanical housings and integration of the electrical components, was completed over the summer of 1999 (again with the help of summer students at TRIUMF). Final testing of the completed bases was carried out in late fall, 1999 and shipment of all the bases (300 units) to TJNAF occurred at the end of calendar year 1999.

The Canadian subgroup is also responsible for the testing and characterizing of all of the photomultiplier tubes to be used with the TRIUMF/$G0$ high-rate bases. With the help of summer students at TJNAF, the primary testing and characterization of all 300 PMTs was completed in late summer, 1998. Further tests will be carried out, with the final bases in place, at TJNAF in early 2000.

The cryostat exit detector array

For the backward angle measurements during the second phase of the $G0$ experiment, simulation results indicate that the elastic and inelastic electrons will be more cleanly separated with the addition of a second array of scintillation detectors, located near the spectrometer-cryostat exit windows. The geometry of these cryostat exit detector (CED) arrays has been studied in detail, and a reference design was completed in the spring. Due to the resident expertise at TRIUMF in producing high quality scintillation detectors and lightguides, the Canadian subgroup has been asked to play a main role in the prototyping and production of the CEDs. A set of prototypes was built at TRIUMF and delivered to Louisiana Tech for further studies in early summer (see Fig. 30). Results from these studies indicate that the reference design and the prototype detectors will meet the specification requirements for the CED arrays.

Full scale production of the CEDs is expected to begin at TRIUMF in early 2000, after the final release of the CED design. The CEDs will also make use of the same types of photomultiplier tubes and specialized TRIUMF/$G0$ bases as the focal-plane detectors.

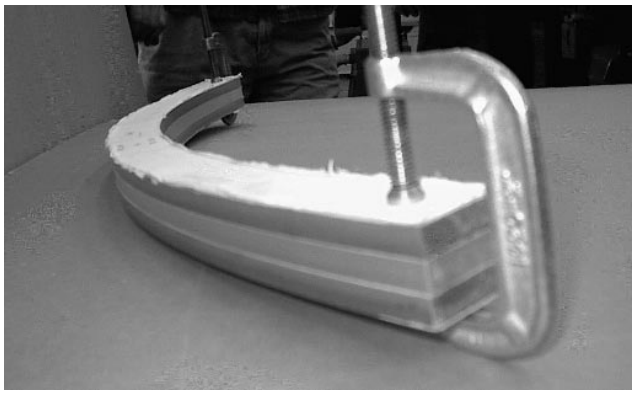

Fig. 30. Prototype CED scintillator element 2, produced at TRIUMF, sandwiched between 2 lexan guard pieces. A pair of 1.5 m long helical-bent lightguides (not shown here), also produced at TRIUMF, transport the light from the scintillator to the photomultiplier tubes.

Resonant cavity position and current monitors

Five sets of XYQ monitors will be required in order to measure the beam current (charge) and trajectory (positions and angles) at several critical locations (directly upstream of the target, at an upstream dispersed focus, and further upstream in the beam line). The proposed current monitor will be of the resonant cavity type, a cylindrical cavity operating in the TM010 mode at 1497 MHz. A beam current sensitivity of $\pm 4 \times 10^{-5}$ measured in a 33 ms integration-time sample will be required to monitor and correct for possible helicity correlated intensity modulations. For the beam position monitors (BPM), a spatial resolution of better than 25 μm at an integration time of 33 ms will be required. Two types of devices will be used: (1) stripline monitors operating in a special switched electrode electronics (SEE) mode; and (2) pairs of cylindrical resonant cavities (X and Y) operating in the TM110 mode.

The beam current and the stripline position monitors were tested during an engineering run in July, 1997 at TJNAF. The run was organized by members of the $G0$ Canadian subgroup and personnel from TJNAF (Hall C), with much of the readout electronics provided by the Canadian subgroup. Precision analog subtractor/divider modules and voltage-to-frequency converters from the TRIUMF parity experiment were readily adapted to the TJNAF beam monitors. Helicity correlated properties of the TJNAF polarized electron beam and noise characteristics of some of the beam monitors were successfully measured. Analysis of the data indicates that the beam current monitors will meet the specification requirements of $\Delta Q/Q \leq 4 \times 10^{-5}$ (in 33 ms). The stripline SEE monitors were able to provide position determinations with $\Delta X \leq 1$ μm (in

33 ms), which will also meet the specification requirements. Further test-beam time is planned for the future.

To read out the analog signals from the beam current and position monitors, and to provide feedback control signals, specialized parity-type electronics will be required for the $G0$ experiment. Much of this electronics, such as precision analog subtractors/dividers and precision voltage-to-frequency converters, has already been designed and used by members of the Canadian subgroup in their parity experiments at TRIUMF. Modifications, driven by the requirements of the $G0$ experiment, were made to some of these electronics modules and they were operated successfully at the July, 1997 engineering run at TJNAF, as mentioned above. Since that time, several voltage-to-frequency converters of the TRIUMF/parity variety have been requested by TJNAF for the $G0$ experiment. Construction of these 32-channel precision V-to-Fs was completed at TRIUMF and delivery made to TJNAF in early 1998. With the successful implementation of these first sets of converters, a second set of V-to-F modules was requested by TJNAF in summer, 1999. This second set of V-to-F modules was again constructed at TRIUMF and delivered to TJNAF in fall, 1999.

Magnetic field measuring apparatus

An automated field measuring apparatus will be used to provide a magnetic verification of the $G0$ superconducting toroid by determining the locations of a pre-specified set of magnetic reference points. These reference points correspond to the zero-crossing locations of specific field components at selected points of symmetry around the toroidal magnet. This measurement will be carried out by scanning a predefined set of contour lines, and determining where specific field components reverse signs. The system must be capable of providing a position determination of 0.2 mm and a field determination of 0.2 G.

Over the past year, considerable effort has gone into the design of this magnetic field measuring apparatus or magnetic verification device at TRIUMF. Due to changes in the design of the $G0$ spectrometer cryostat, the conceptual design for the magnetic verification device has itself gone through 3 iterations. The present design concept is shown in Fig. 31. The proposed device will consist of a programmable gantry with full 3D motion anywhere within a 4 m $\times$ 4 m $\times$ 2 m region. A set of high precision Hall probes is mounted at the end of a probe boom on the gantry. This system has been designed so that it will be capable of motion in either (x, y, z) or (r, θ, z), via a set of interchangable probe booms. A detailed parts list has been generated for the present design, finite-element deflection and stability studies have been carried out, and a

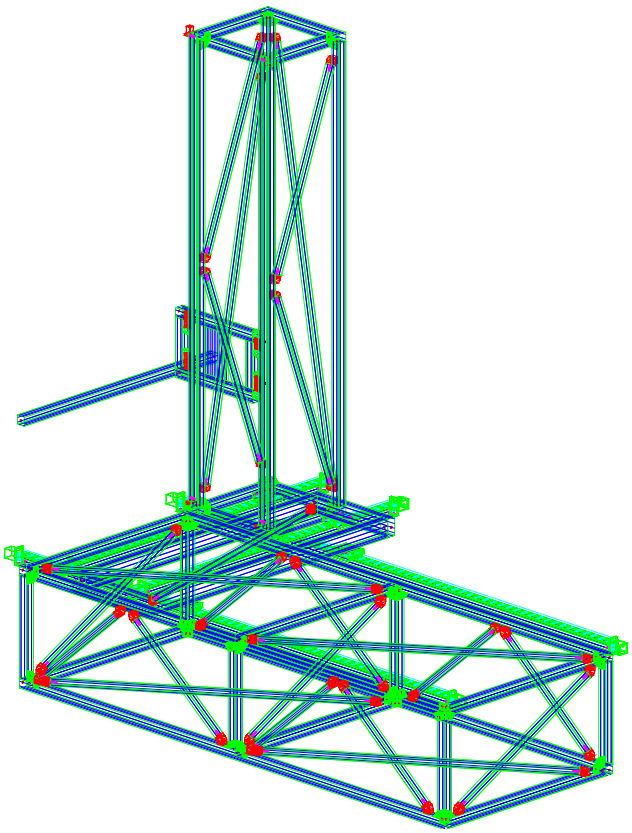

Fig. 31. Conceptual layout of the magnetic verification apparatus.

TRIUMF/$G0$ Design Note detailing this design has been produced [$G0$ internal report, $G0$-99-050]. Procurement of parts commenced in late fall, with assembly and testing expected to begin in spring, 2000.

Although this magnetic verification device is being designed, tested and built by the Canadian subgroup at TRIUMF and the University of Manitoba, it should be noted that financial support for all hardware components of this subsystem will be provided via NSF funding for $G0$ through the University of Illinois.

Neutron background studies

A set of measurements is being devised to determine the neutron background and energy spectrum in the vicinity of the $G0$ detector system. This effort is being coordinated by the Canadian subgroup (with help from members of the TRIUMF Safety Group) and personnel from TJNAF (Hall C). The present set of proposed measurements makes use of a Multisphere (Bonner sphere) detector system, which is capable of determining the neutron energy spectrum at specific locations. The Multisphere detector consists of a ^{6}LiI(Eu) scintillation counter system, used in conjunction with a set of moderating polyethylene spheres [Moritz *et al.*, Health Physics **58**, 487 (1990)]. Neutron

rates/yields are measured via the neutron capture reaction $^6\mathrm{Li}(n,\alpha)t$ in the scintillator, under different moderating sphere configurations. The underlying neutron energy spectrum can then be unfolded from the set of yield measurements.

Test beam time in Hall C was made available in December, and a first set of neutron background measurements using the Multisphere detector(s) was carried out. Results from this test run are presently being analyzed and preliminary results will be available shortly. Further test beam time is planned for the future. Presently, one Multisphere detector system exists at TRIUMF and was made available for this measurement. Current plans are to build 2 more LiI(Eu) scintillation counters to enable the studies to be completed in a timely manner.

Canadian subgroup of the *G*0 collaboration: J. Birchall, W.R. Falk, L. Lee, S.A. Page, W.D. Ramsay, W.T.H. van Oers, R.J. Woo (Manitoba); E. Korkmaz, T. Porcelli (Northern British Columbia); C.A. Davis (TRIUMF).